

# Pathwise Conditioning of Gaussian Processes

**James T. Wilson\***

*Imperial College London*

J.WILSON17@IMPERIAL.AC.UK

**Viacheslav Borovitskiy\***

*St. Petersburg State University and*

*St. Petersburg Department of Steklov Mathematical Institute of Russian Academy of Sciences*

VIACHESLAV.BOROVITSKIY@GMAIL.COM

**Alexander Terenin\***

*Imperial College London*

A.TERENIN17@IMPERIAL.AC.UK

**Peter Mostowsky\***

*St. Petersburg State University*

PMOSTOWSKY@GMAIL.COM

**Marc Peter Deisenroth**

*Centre for Artificial Intelligence, University College London*

M.DEISENROTH@UCL.AC.UK

**Editor:** Kilian Weinberger

## Abstract

As Gaussian processes are used to answer increasingly complex questions, analytic solutions become scarcer and scarcer. Monte Carlo methods act as a convenient bridge for connecting intractable mathematical expressions with actionable estimates via sampling. Conventional approaches for simulating Gaussian process posteriors view samples as draws from marginal distributions of process values at finite sets of input locations. This distribution-centric characterization leads to generative strategies that scale cubically in the size of the desired random vector. These methods are prohibitively expensive in cases where we would, ideally, like to draw high-dimensional vectors or even continuous sample paths. In this work, we investigate a different line of reasoning: rather than focusing on distributions, we articulate Gaussian conditionals at the level of random variables. We show how this *pathwise* interpretation of conditioning gives rise to a general family of approximations that lend themselves to efficiently sampling Gaussian process posteriors. Starting from first principles, we derive these methods and analyze the approximation errors they introduce. We, then, ground these results by exploring the practical implications of pathwise conditioning in various applied settings, such as global optimization and reinforcement learning.

**Keywords:** Gaussian processes, approximate posteriors, efficient sampling.

## 1. Introduction

In machine learning, the narrative of Gaussian processes (GPs) is dominated by talk of distributions (Rasmussen and Williams, 2006). This view is often helpful and convenient: a Gaussian process is a random function; however, seeing as we may trivially marginalize out arbitrary subsets of this function, we can simply focus on its behavior at a finite number of input locations. When dealing with regression and classification problems, this

---

\*Equal contribution.

reduction simplifies discourse and expedites implementation by allowing us to work with joint distributions at training and test locations instead of random functions.

Model-based learning and prediction generally service broader goals. For example, when making decisions in the face of uncertainty, models enable us to simulate the consequences of our actions. Decision-making, then, amounts to optimizing the expectation of a simulated quantity of interest, such as a cost or a reward. Be it for purposes of safety or for balancing trade-offs between long-term and short-term goals, it is crucial that these simulations faithfully portray both knowledge and uncertainty. Gaussian processes are known to make accurate, well-calibrated predictions and, therefore, stand as the model-of-choice in fields such as Bayesian optimization (Shahriari et al., 2015), uncertainty quantification (Bect et al., 2012), and model-based reinforcement learning (Deisenroth et al., 2015).

Unfortunately, marginal distributions and simulations do not always go hand in hand. When the quantity of interest is a function of a process value  $f(\mathbf{x}_*)$  at an individual input location  $\mathbf{x}_*$ , its expectation can sometimes be obtained analytically. Conversely, when this quantity is a function of process values  $\mathbf{f}_* = f(\mathbf{X}_*)$  at multiple locations  $\mathbf{X}_*$ , its expectation is generally intractable. Rather than solving these integrals directly in terms of marginal distributions  $p(\mathbf{f}_*)$ , we therefore estimate them by averaging over many simulations of  $\mathbf{f}_*$ . Drawing  $\mathbf{f}_*$  from  $p(\mathbf{f}_*)$  takes  $\mathcal{O}(*^3)$  time, where  $*$  is the number of input locations. Hence, distribution-based approaches to sampling  $\mathbf{f}_*$  quickly become untenable as this number increases. In these cases, we may be better off thinking about GPs from a perspective that naturally lends itself to sampling

In the early 1970s, one such view surfaced in the then nascent field of geostatistics (Journel and Huijbregts, 1978; Chilès and Delfiner, 2012). Instead of emphasizing the statistical properties of Gaussian random variables, “conditioning by Kriging” encourages us to think in terms of the variables themselves. We study the broader implications of this paradigm shift to develop a general framework for conditioning Gaussian processes at the level of random functions. Formulating conditioning in terms of sample paths, rather than distributions, allows us to separate out the effect of the prior from that of the data. By leveraging this property, we can use *pathwise conditioning* to efficiently approximate function draws from GP posteriors. As we will see, working with sample paths enables us to simulate process values  $\mathbf{f}_*$  in  $\mathcal{O}(*)$  time and brings with it a host of additional benefits.

The structure of the remaining text is as follows. Section 2 and Section 3 introduce pathwise conditioning of Gaussian random vectors and processes, respectively. Section 4 surveys strategies for approximating function draws from GP priors, while Section 5 discusses methods for mapping from prior to posterior random variables. Section 6 studies the behavior of errors introduced by different approximation techniques, and Section 7 complements this theory with a bit of empiricism by exploring a number of examples. Section 8 concludes.

**Notation** By way of example, we denote matrices as  $\mathbf{A}$  and vectors as  $\mathbf{a}$ . We write  $\mathbf{x} = \mathbf{a} \oplus \mathbf{b}$  for the direct sum (i.e. concatenation) of vectors  $\mathbf{a}$  and  $\mathbf{b}$ . Throughout, we use  $|\cdot|$  to denote the cardinality of sets and dimensionality of vectors. When dealing with covariance matrices  $\Sigma = \text{Cov}(\mathbf{x}, \mathbf{x})$ , we use subscripts to identify corresponding blocks. For example,  $\Sigma_{\mathbf{a}, \mathbf{b}} = \text{Cov}(\mathbf{a}, \mathbf{b})$ . As shorthand, we denote the evaluation of a function  $f : \mathcal{X} \rightarrow \mathbb{R}$  at a finite set of locations  $\mathbf{X}_* \subset \mathcal{X}$  by the vector  $\mathbf{f}_*$ . Putting these together, when dealing with random variables  $\mathbf{f}_* = f(\mathbf{X}_*)$  and  $\mathbf{f}_n = f(\mathbf{X}_n)$ , we write  $\mathbf{K}_{*,n} = \text{Cov}(\mathbf{f}_*, \mathbf{f}_n)$ .

## 2. Conditioning Gaussian distributions and random vectors

A random vector  $\mathbf{x} = (x_1, \dots, x_n) \in \mathbb{R}^n$  is said to be Gaussian if there exists a matrix  $\mathbf{L}$  and vector  $\boldsymbol{\mu}$  such that

$$\mathbf{x} \stackrel{d}{=} \boldsymbol{\mu} + \mathbf{L}\boldsymbol{\zeta} \quad \boldsymbol{\zeta} \sim \mathcal{N}(\mathbf{0}, \mathbf{I}), \quad (1)$$

where  $\mathcal{N}(\mathbf{0}, \mathbf{I})$  is the standard (multivariate) normal distribution, the probability density function of which is given below. Each such distribution is uniquely identified by its first two moments: its mean  $\boldsymbol{\mu} = \mathbb{E}(\mathbf{x})$  and its covariance  $\boldsymbol{\Sigma} = \mathbb{E}[(\mathbf{x} - \boldsymbol{\mu})(\mathbf{x} - \boldsymbol{\mu})^\top]$ . Assuming it exists, the corresponding density function is defined as

$$p(\mathbf{x}) = \mathcal{N}(\mathbf{x} \mid \boldsymbol{\mu}, \boldsymbol{\Sigma}) = \frac{1}{\sqrt{|2\pi\boldsymbol{\Sigma}|}} \exp\left(-\frac{1}{2}(\mathbf{x} - \boldsymbol{\mu})^\top \boldsymbol{\Sigma}^{-1}(\mathbf{x} - \boldsymbol{\mu})\right). \quad (2)$$

The representation of  $\mathbf{x}$  given by (1) is commonly referred to as its *location-scale* form and stands as the most widely used method for generating Gaussian random vectors. Since  $\boldsymbol{\zeta}$  has identity covariance, any matrix square root of  $\boldsymbol{\Sigma}$ , such as its Cholesky factor  $\mathbf{L}$  with  $\boldsymbol{\Sigma} = \mathbf{L}\mathbf{L}^\top$ , may be used to draw  $\mathbf{x}$  as prescribed by (1).

Here, we focus on multivariate cases  $n > 1$  and investigate different ways of reasoning about random variables  $\mathbf{a} \mid \mathbf{b} = \boldsymbol{\beta}$  for non-trivial partitions  $\mathbf{x} = \mathbf{a} \oplus \mathbf{b}$ .

### 2.1 Distributional conditioning

The quintessential approach to deriving the distribution of  $\mathbf{a}$  subject to the condition  $\mathbf{b} = \boldsymbol{\beta}$  begins by employing the usual set of matrix identities to factor  $p(\mathbf{b})$  from  $p(\mathbf{a}, \mathbf{b})$ . Applying Bayes' rule,  $p(\mathbf{b})$  then cancels out and  $p(\mathbf{a} \mid \mathbf{b} = \boldsymbol{\beta})$  is identified as the remaining term—namely, the Gaussian distribution  $\mathcal{N}(\boldsymbol{\mu}_{\mathbf{a}|\boldsymbol{\beta}}, \boldsymbol{\Sigma}_{\mathbf{a},\mathbf{a}|\boldsymbol{\beta}})$  with moments

$$\boldsymbol{\mu}_{\mathbf{a}|\boldsymbol{\beta}} = \boldsymbol{\mu}_{\mathbf{a}} + \boldsymbol{\Sigma}_{\mathbf{a},\mathbf{b}}\boldsymbol{\Sigma}_{\mathbf{b},\mathbf{b}}^{-1}(\boldsymbol{\beta} - \boldsymbol{\mu}_{\mathbf{b}}) \quad \boldsymbol{\Sigma}_{\mathbf{a},\mathbf{a}|\boldsymbol{\beta}} = \boldsymbol{\Sigma}_{\mathbf{a},\mathbf{a}} - \boldsymbol{\Sigma}_{\mathbf{a},\mathbf{b}}\boldsymbol{\Sigma}_{\mathbf{b},\mathbf{b}}^{-1}\boldsymbol{\Sigma}_{\mathbf{b},\mathbf{a}}. \quad (3)$$

Having obtained this conditional distribution, we can now generate  $\mathbf{a} \mid \mathbf{b} = \boldsymbol{\beta}$  by computing a matrix square root of  $\boldsymbol{\Sigma}_{\mathbf{a},\mathbf{a}|\boldsymbol{\beta}}$  and constructing a location-scale transform (1).

Due to their emphasis of conditional distributions, we refer to methods that represent or generate a random variable  $\mathbf{a} \mid \mathbf{b} = \boldsymbol{\beta}$  by way of  $p(\mathbf{a} \mid \mathbf{b} = \boldsymbol{\beta})$  as being *distributional* in kind. This approach to conditioning is not only standard, but particularly natural when quantities of interest may be derived analytically from  $p(\mathbf{a} \mid \mathbf{b} = \boldsymbol{\beta})$ . Many quantities, such as expectations of nonlinear functions, cannot be deduced analytically from  $p(\mathbf{a} \mid \mathbf{b} = \boldsymbol{\beta})$  alone, however. In these case, we must instead work with realizations of  $\mathbf{a} \mid \mathbf{b} = \boldsymbol{\beta}$ . Since the cost of obtaining a matrix square root of  $\boldsymbol{\Sigma}_{\mathbf{a},\mathbf{a}|\boldsymbol{\beta}}$  scales cubically in  $|\mathbf{a}|$ , distributional approaches to evaluating these quantities struggle to accommodate high-dimensional random vectors. To address this issue, we now consider Gaussian conditioning in another light.

### 2.2 Pathwise conditioning

Instead of taking a *distribution-first* stance on Gaussian conditionals, we may think of conditioning directly in terms of random variables. In this *variable-first* paradigm, we will explicitly map samples from the prior to draws from a posterior and let the corresponding

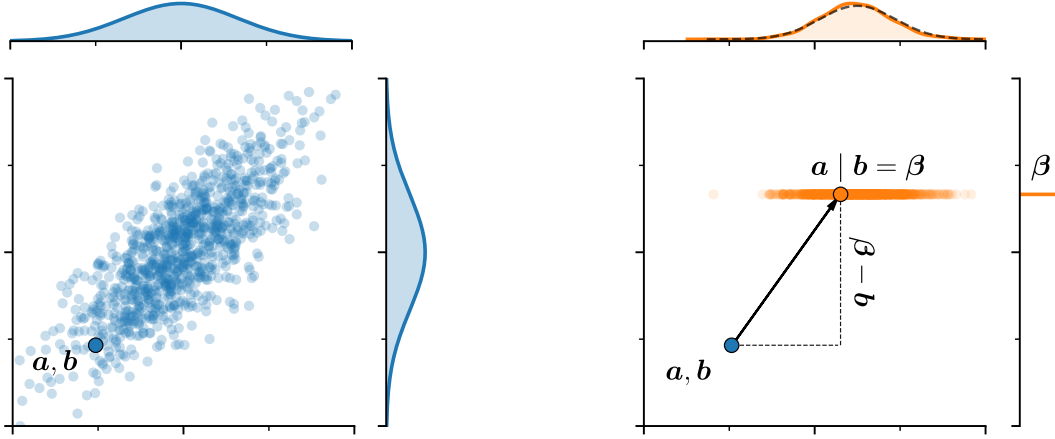


Figure 1: Visualization of Matheron’s update rule for a bivariate normal distribution with correlation coefficient  $\rho = 0.75$ . *Left*: Draws from  $p(\mathbf{a}, \mathbf{b})$  are shown alongside the marginal distributions of  $\mathbf{a}$  and  $\mathbf{b}$ . *Right*: Theorem 1 is used to update samples shown on the left subject to the condition  $\mathbf{b} = \beta$ . This process is illustrated in full for a particular draw. *Top right*: the empirical distribution of the update samples is compared with  $p(\mathbf{a} \mid \mathbf{b} = \beta)$ .

relationship between distributions follow implicitly. Throughout this work, we investigate this notion of *pathwise conditioning* through the lens of the following result.

**Theorem 1 (Matheron’s Update Rule)** *Let  $\mathbf{a}$  and  $\mathbf{b}$  be jointly Gaussian, centered random variables. Then, the random variable  $\mathbf{a}$  conditional on  $\mathbf{b} = \beta$  may be expressed as*

$$(\mathbf{a} \mid \mathbf{b} = \beta) \stackrel{d}{=} \mathbf{a} + \Sigma_{\mathbf{a},\mathbf{b}} \Sigma_{\mathbf{b},\mathbf{b}}^{-1} (\beta - \mathbf{b}). \quad (4)$$

**Proof** Comparing the mean and covariance on both sides immediately affirms the result

$$\begin{aligned} \mathbb{E}(\mathbf{a} + \Sigma_{\mathbf{a},\mathbf{b}} \Sigma_{\mathbf{b},\mathbf{b}}^{-1} (\beta - \mathbf{b})) &= \mu_{\mathbf{a}} + \Sigma_{\mathbf{a},\mathbf{b}} \Sigma_{\mathbf{b},\mathbf{b}}^{-1} (\beta - \mu_{\mathbf{b}}) \\ &= \mathbb{E}(\mathbf{a} \mid \mathbf{b} = \beta) \end{aligned} \quad \begin{aligned} \text{Cov}(\mathbf{a} + \Sigma_{\mathbf{a},\mathbf{b}} \Sigma_{\mathbf{b},\mathbf{b}}^{-1} (\beta - \mathbf{b})) &= \Sigma_{\mathbf{a},\mathbf{a}} + \Sigma_{\mathbf{a},\mathbf{b}} \Sigma_{\mathbf{b},\mathbf{b}}^{-1} \Sigma_{\mathbf{b},\mathbf{b}} \Sigma_{\mathbf{b},\mathbf{b}}^{-1} \Sigma_{\mathbf{b},\mathbf{a}} - 2 \Sigma_{\mathbf{a},\mathbf{b}} \Sigma_{\mathbf{b},\mathbf{b}}^{-1} \Sigma_{\mathbf{b},\mathbf{a}} \\ &= \Sigma_{\mathbf{a},\mathbf{a}} - \Sigma_{\mathbf{a},\mathbf{b}} \Sigma_{\mathbf{b},\mathbf{b}}^{-1} \Sigma_{\mathbf{b},\mathbf{a}} = \text{Cov}(\mathbf{a} \mid \mathbf{b} = \beta). \end{aligned} \quad (5)$$

■

This observation leads to a straightforward, alternative recipe for generating  $\mathbf{a} \mid \mathbf{b} = \beta$ : first, draw  $\mathbf{a}, \mathbf{b} \sim p(\mathbf{a}, \mathbf{b})$ ; then, update this sample according to (4). Compared to the location-scale approach discussed in Section 2.1, a key difference is that we now sample *before* conditioning, rather than after. Figure 1 visualizes the deterministic process of updating previously generated draws from the prior subject to the condition  $\mathbf{b} = \beta$ .

At first glance, Matheron’s update rule may seem more like an interesting footnote than a valuable tool. Indeed, the conventional strategy for sampling  $\mathbf{a}, \mathbf{b}$  (which requires us to take a matrix square root of  $\Sigma$ ) is more expensive than that for generating  $\mathbf{a} \mid \mathbf{b} = \beta$ . We

will discuss this matter in detail in the later sections. For now, however, let us strengthen our intuition by delving deeper into this theorem's function-analytic origins.

### 2.3 Deriving pathwise conditioning via conditional expectations

Here, we overview the precise formalism that gives rise to the pathwise approach to conditioning Gaussian random variables and show how to *derive* this result from first principles. Throughout this section, we take  $\mathbf{a} \in \mathbb{R}^m$  and  $\mathbf{b} \in \mathbb{R}^n$  to be centered random vectors defined on the same probability space.

The core idea is to decompose  $\mathbf{a}$  as the sum of two independent terms—one that depends on  $\mathbf{b}$  and one that does not—and represent  $\mathbf{a} \mid \mathbf{b} = \boldsymbol{\beta}$  by conditioning both terms on  $\mathbf{b} = \boldsymbol{\beta}$ . We first prove that conditioning this additive decomposition of  $\mathbf{a}$  is simple and intuitive.

**Lemma 2** *Consider three random vectors  $\mathbf{a} \in \mathbb{R}^m$ ,  $\mathbf{b} \in \mathbb{R}^n$ ,  $\mathbf{c} \in \mathbb{R}^m$  such that*

$$\mathbf{a} \stackrel{\text{d}}{=} f(\mathbf{b}) + \mathbf{c}, \quad (6)$$

*where  $f$  is a measurable function of  $\mathbf{b}$  and where  $\mathbf{b}$  is independent of  $\mathbf{c}$ . Then,*

$$(\mathbf{a} \mid \mathbf{b} = \boldsymbol{\beta}) \stackrel{\text{d}}{=} f(\boldsymbol{\beta}) + \mathbf{c}. \quad (7)$$

**Proof** Let  $\pi_{\mathbf{x}}$  denote the distribution of a generic random variable  $\mathbf{x}$ . Further, let  $\pi_{\mathbf{a}|\mathbf{b}}(\cdot \mid \cdot)$  be the (regular) conditional probability measure given by disintegration<sup>1</sup> of  $(\mathbf{a}, \mathbf{b})$ , such that

$$\int_B \pi_{\mathbf{a}|\mathbf{b}}(A \mid \boldsymbol{\beta}) d\pi_{\mathbf{b}}(\boldsymbol{\beta}) = \mathbb{P}(\mathbf{a} \in A, \mathbf{b} \in B) \quad (8)$$

for measurable sets  $A \subseteq \mathbb{R}^m$ ,  $B \subseteq \mathbb{R}^n$ . When  $\mathbf{a} \mid \mathbf{b} = \boldsymbol{\beta}$  is represented per (7), we have

$$\begin{aligned} \int_B \mathbb{P}(f(\boldsymbol{\beta}) + \mathbf{c} \in A) d\pi_{\mathbf{b}}(\boldsymbol{\beta}) &= \int_B \left( \int_{\mathbb{R}^m} \mathbb{1}_{\{f(\boldsymbol{\beta}) + \boldsymbol{\varsigma} \in A\}} d\pi_{\mathbf{c}}(\boldsymbol{\varsigma}) \right) d\pi_{\mathbf{b}}(\boldsymbol{\beta}) \\ &= \int_{\mathbb{R}^m \times \mathbb{R}^n} \mathbb{1}_{\{f(\boldsymbol{\beta}) + \boldsymbol{\varsigma} \in A, \boldsymbol{\beta} \in B\}} d\pi_{\mathbf{b}, \mathbf{c}}(\boldsymbol{\beta}, \boldsymbol{\varsigma}) \\ &= \mathbb{P}(f(\mathbf{b}) + \mathbf{c} \in A, \mathbf{b} \in B) = \mathbb{P}(\mathbf{a} \in A, \mathbf{b} \in B), \end{aligned} \quad (9)$$

where we have begun by expressing probabilities as integrals of indicator functions, before using Tonelli's theorem and independence to express the iterated integral as the double integral over the joint probability measure  $\pi_{\mathbf{b}, \mathbf{c}}(\boldsymbol{\beta}, \boldsymbol{\varsigma})$ . Comparing the left-hand sides of (8) and (9) affirms the claim.  $\blacksquare$

In words, Lemma 2 tells us that for suitably chosen functions  $f$ , the act of conditioning  $\mathbf{a}$  on  $\mathbf{b} = \boldsymbol{\beta}$  amounts to adding an random variable  $\mathbf{c}$  to a deterministic transformation  $f(\boldsymbol{\beta})$  of the outcome  $\boldsymbol{\beta}$ . For this statement to hold, we require the *residual*  $\mathbf{c} = \mathbf{a} - f(\mathbf{b})$  induced by  $f$  to be independent of  $\mathbf{b}$ . Fortunately, such a function  $f$  is well-known in the special case of jointly Gaussian random variables—namely, the *conditional expectation*  $f : \mathbf{b} \mapsto \mathbb{E}(\mathbf{a} \mid \mathbf{b})$ .

1. See discussion and details on disintegration by Chang and Pollard (1997) and Kallenberg (2006).

For square-integrable random variables, the conditional expectation of  $\mathbf{a}$  given  $\mathbf{b}$  is defined as the (almost surely) unique solution to the minimization problem

$$\mathbb{E}(\mathbf{a} \mid \mathbf{b}) = \arg \min_{f \in \mathcal{F}} \mathbb{E} \|\mathbf{a} - f(\mathbf{b})\|^2, \quad (10)$$

where  $\mathcal{F}$  denotes the set of all Borel-measurable functions  $f : \mathbb{R}^n \rightarrow \mathbb{R}^m$  (Kallenberg, 2006, Chapter 6). Put simply,  $\mathbb{E}(\mathbf{a} \mid \mathbf{b})$  is the measurable function of  $\mathbf{b}$  that best predicts  $\mathbf{a}$  in the sense of minimizing the mean-square error (10). This characterization of the conditional expectation is equivalent to defining it as the orthogonal projection of  $\mathbf{a}$  onto the  $\sigma$ -algebra generated by  $\mathbf{b}$ , denoted  $\sigma(\mathbf{b})$ . Consequently, a necessary and sufficient condition for  $\mathbb{E}(\mathbf{a} \mid \mathbf{b}) \in \mathcal{F}$  to uniquely solve (10) is that the residual  $\mathbf{c} = \mathbf{a} - \mathbb{E}(\mathbf{a} \mid \mathbf{b})$  be orthogonal to all  $\sigma(\mathbf{b})$ -measurable random variables (Luenberger, 1997, page 50). Here, *orthogonality* can be understood as the absence of correlation, which (for jointly Gaussian random variables) implies independence. As a result, we may satisfy the assumptions of Lemma 2 by writing

$$\mathbf{a} = \mathbb{E}(\mathbf{a} \mid \mathbf{b}) + \mathbf{c}, \quad (11)$$

such that  $\mathbf{a}$  decomposes into a function of  $\mathbf{b}$  and an independent variable  $\mathbf{c} = \mathbf{a} - \mathbb{E}(\mathbf{a} \mid \mathbf{b})$ .

As a final remark, we may also use these principles to concisely derive the conditional expectation for jointly Gaussian random variables. For now, suppose that the conditional expectation is a linear function of  $\mathbf{b}$ , i.e. that  $\mathbb{E}(\mathbf{a} \mid \mathbf{b}) = \mathbf{S}\mathbf{b}$  for some matrix  $\mathbf{S} \in \mathbb{R}^{m \times n}$ . To satisfy the orthogonality condition of (10), we require  $\text{Cov}(\mathbf{a} - \mathbf{S}\mathbf{b}, \mathbf{b}) = \mathbf{0}$ , implying that  $\Sigma_{\mathbf{a}, \mathbf{b}} - \mathbf{S}\Sigma_{\mathbf{b}, \mathbf{b}} = \mathbf{0}$ . Rearranging terms and solving for  $\mathbf{S}$  gives  $\mathbf{S} = \Sigma_{\mathbf{a}, \mathbf{b}}\Sigma_{\mathbf{b}, \mathbf{b}}^{-1}$ . With this expression in hand, to show that linearity was assumed without loss of generality, write  $\mathbf{a} = \mathbf{S}\mathbf{b} + \mathbf{a} - \mathbf{S}\mathbf{b}$ , which we may express as  $\mathbf{a} = \mathbf{S}\mathbf{b} + \mathbf{c}$ . Taking the conditional expectation of both sides, we may directly calculate  $\mathbb{E}(\mathbf{a} \mid \mathbf{b})$  by writing

$$\mathbb{E}(\mathbf{a} \mid \mathbf{b}) = \mathbb{E}(\mathbf{S}\mathbf{b} + \mathbf{c} \mid \mathbf{b}) = \underbrace{\mathbb{E}(\mathbf{S}\mathbf{b} \mid \mathbf{b})}_{\mathbf{S}\mathbf{b}} + \underbrace{\mathbb{E}(\mathbf{c})}_{\mathbf{0}} = \Sigma_{\mathbf{a}, \mathbf{b}}\Sigma_{\mathbf{b}, \mathbf{b}}^{-1}\mathbf{b}, \quad (12)$$

where we have used linearity of conditional expectation, followed by independence of  $\mathbf{c}$  and  $\mathbf{b}$  to go from the second to the third expression. We now revisit Theorem 1.

**Theorem 1 (Matheron's Update Rule)** *Let  $\mathbf{a}$  and  $\mathbf{b}$  be jointly Gaussian, centered random vectors. Then, the random vector  $\mathbf{a}$  conditional on  $\mathbf{b} = \boldsymbol{\beta}$  may be expressed as*

$$(\mathbf{a} \mid \mathbf{b} = \boldsymbol{\beta}) \stackrel{\text{d}}{=} \mathbf{a} + \Sigma_{\mathbf{a}, \mathbf{b}}\Sigma_{\mathbf{b}, \mathbf{b}}^{-1}(\boldsymbol{\beta} - \mathbf{b}). \quad (4)$$

**Proof** With  $\mathbf{c} = \mathbf{a} - \Sigma_{\mathbf{a}, \mathbf{b}}\Sigma_{\mathbf{b}, \mathbf{b}}^{-1}\mathbf{b}$ , begin by writing

$$\mathbf{a} = \mathbb{E}(\mathbf{a} \mid \mathbf{b}) + (\mathbf{a} - \mathbb{E}(\mathbf{a} \mid \mathbf{b})) = \Sigma_{\mathbf{a}, \mathbf{b}}\Sigma_{\mathbf{b}, \mathbf{b}}^{-1}\mathbf{b} + \mathbf{c}. \quad (13)$$

Since  $\mathbf{b}$  and  $\mathbf{c}$  are jointly Gaussian but uncorrelated, it follows that they are independent. Setting  $f(\mathbf{b}) = \Sigma_{\mathbf{a}, \mathbf{b}}\Sigma_{\mathbf{b}, \mathbf{b}}^{-1}\mathbf{b}$  and using Lemma 2 to condition both sides on  $\mathbf{b} = \boldsymbol{\beta}$  gives

$$(\mathbf{a} \mid \mathbf{b} = \boldsymbol{\beta}) \stackrel{\text{d}}{=} \Sigma_{\mathbf{a}, \mathbf{b}}\Sigma_{\mathbf{b}, \mathbf{b}}^{-1}\boldsymbol{\beta} + (\mathbf{a} - \Sigma_{\mathbf{a}, \mathbf{b}}\Sigma_{\mathbf{b}, \mathbf{b}}^{-1}\mathbf{b}) = \mathbf{a} + \Sigma_{\mathbf{a}, \mathbf{b}}\Sigma_{\mathbf{b}, \mathbf{b}}^{-1}(\boldsymbol{\beta} - \mathbf{b}). \quad (14)$$

Hence, the claim follows. ■

In summary, we have shown that Matheron’s update rule (Theorem 1) is a direct consequence of the fact that a Gaussian random variable  $\mathbf{a}$  conditioned on the outcome  $\beta$  of another (jointly) Gaussian random variable  $\mathbf{b}$  may be expressed as the sum of two independent terms: the conditional expectation  $\mathbb{E}(\mathbf{a} \mid \mathbf{b} = \beta)$  evaluated at  $\beta$  and the residual  $\mathbf{c} = \mathbf{a} - \mathbb{E}(\mathbf{a} \mid \mathbf{b})$ . Rearranging these terms gives (4).

With these ideas in mind, we are now ready to explore this work’s primary theme: Matheron’s update rule enables us to decompose  $\mathbf{a} \mid \mathbf{b} = \beta$  into the prior random variable  $\mathbf{a}$  and a data-driven update  $\Sigma_{\mathbf{a},\mathbf{b}}\Sigma_{\mathbf{b},\mathbf{b}}^{-1}(\beta - \mathbf{b})$  that explicitly corrects for the error in the coinciding value of  $\mathbf{b}$  given the condition  $\mathbf{b} = \beta$ . Hence, Theorem 1 provides an explicit means of separating out the influence of the prior from that of the data. We now proceed to investigate the implications of pathwise conditioning for Gaussian processes.

### 3. Conditioning Gaussian processes and random functions

A Gaussian process (GP) is a random function  $f : \mathcal{X} \rightarrow \mathbb{R}$ , such that, for any finite collection of points  $\mathbf{X} \subset \mathcal{X}$ , the random vector  $\mathbf{f} = f(\mathbf{X})$  follows a Gaussian distribution. Such a process is uniquely identified by a mean function  $\mu : \mathcal{X} \rightarrow \mathbb{R}$  and a positive semi-definite kernel  $k : \mathcal{X} \times \mathcal{X} \rightarrow \mathbb{R}$ . Hence, if  $f \sim \mathcal{GP}(\mu, k)$ , then  $\mathbf{f} \sim \mathcal{N}(\boldsymbol{\mu}, \mathbf{K})$  is multivariate normal with mean  $\boldsymbol{\mu} = \mu(\mathbf{X})$  and covariance  $\mathbf{K} = k(\mathbf{X}, \mathbf{X})$ .

Throughout this section, we investigate different ways of reasoning about the random variable  $\mathbf{f}_* \mid \mathbf{f}_n = \mathbf{y}$  for some non-trivial partition  $\mathbf{f} = \mathbf{f}_n \oplus \mathbf{f}_*$ . Here,  $\mathbf{f}_n = f(\mathbf{X}_n)$  are process values at a set of training locations  $\mathbf{X}_n \subset \mathbf{X}$  where we would like to introduce a condition  $\mathbf{f}_n = \mathbf{y}$ , while  $\mathbf{f}_* = f(\mathbf{X}_*)$  are process values at a set of test locations  $\mathbf{X}_* \subset \mathbf{X}$  where we would like to obtain a random variable  $\mathbf{f}_* \mid \mathbf{f}_n = \mathbf{y}$ . Mirroring Section 2, we begin by reviewing distributional conditioning, before examining its pathwise counterpart.

#### 3.1 Distributional conditioning

As in finite-dimensional cases, we may obtain  $\mathbf{f}_* \mid \mathbf{y}$  by first finding its conditional distribution. Since process values  $(\mathbf{f}_n, \mathbf{f}_*)$  are defined as jointly Gaussian, this procedure closely resembles that of Section 2.1: we factor out the marginal distribution of  $\mathbf{f}_n$  from the joint distribution  $p(\mathbf{f}_n, \mathbf{f}_*)$  and, upon canceling, identify the remaining distribution as  $p(\mathbf{f}_* \mid \mathbf{y})$ . Having done so, we find that the conditional distribution is the Gaussian  $\mathcal{N}(\boldsymbol{\mu}_{*|\mathbf{y}}, \mathbf{K}_{*,*|\mathbf{y}})$  with moments

$$\boldsymbol{\mu}_{*|\mathbf{y}} = \boldsymbol{\mu}_* + \mathbf{K}_{*,n}\mathbf{K}_{n,n}^{-1}(\mathbf{y} - \boldsymbol{\mu}_n) \quad \mathbf{K}_{*,*|\mathbf{y}} = \mathbf{K}_{*,*} - \mathbf{K}_{*,n}\mathbf{K}_{n,n}^{-1}\mathbf{K}_{n,*}. \quad (15)$$

As before, we may now generate  $\mathbf{f}_* \mid \mathbf{y}$  in  $\mathcal{O}(*^3)$  time using a location-scale transform (1).

This strategy for sampling Gaussian process posteriors is subtly different from the one given in Section 2.1. A Gaussian process is a random function, and conditioning on  $\mathbf{f}_n = \mathbf{y}$  does not change this fact. Unfortunately, (conditional) distributions over infinite-dimensional objects can be difficult to manipulate in practice. Distributional approaches, therefore, focus on finite-dimensional subsets  $\mathbf{f} = \mathbf{f}_n \oplus \mathbf{f}_*$ , while marginalizing out the remaining process values. Doing so allows them to perfectly describe the random variable  $\mathbf{f}_* \mid \mathbf{y}$  via its mean and covariance (15).

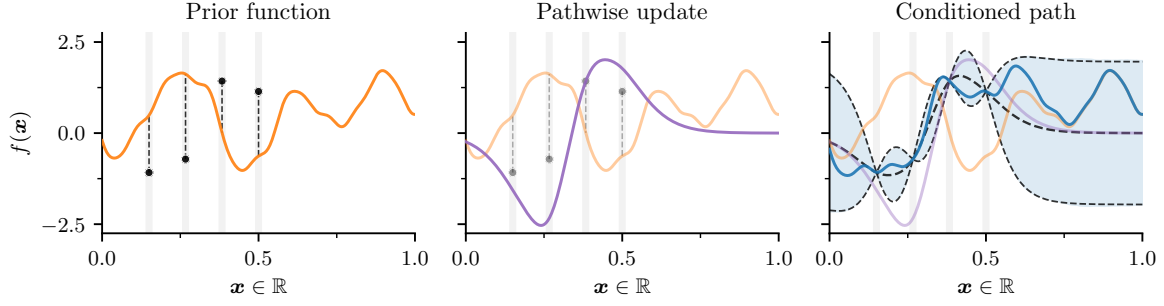


Figure 2: Visual guide for pathwise conditioning of Gaussian processes. *Left:* The residual  $\mathbf{y} - \mathbf{f}_n$  (dashed black) of a draw  $f \sim \mathcal{GP}(0, k)$ , shown in orange, given observations  $\mathbf{y}$  (black). *Middle:* A pathwise update (purple) is constructed in accordance with Corollary 4. *Right:* Prior and update are combined to represent conditional (blue). Empirical moments (light blue) of  $10^5$  conditioned paths are compared with those of the model (dashed black). The sample average, which matches the posterior mean, has been omitted for clarity.

When it comes to sampling  $\mathbf{f}_* \mid \mathbf{y}$ , however, these approaches have clear limitations. As discussed previously, a key issue is that their  $\mathcal{O}(*^3)$  time complexity restricts them to problems that only require us to jointly simulate process values at a manageable number of test locations (up to several thousand). In some senses, this condition is fairly generous. After all, we are often only asked to generate a handful of process values at a time. Still, other problems effectively require us to realize  $f \mid \mathbf{y}$  in its entirety. Similar issues arise when  $\mathbf{X}_*$  is not defined in advance, such as when gradient information is used to adaptively determine the locations at which to jointly sample the posterior. In these cases and more, we would ideally like to sample actual functions that we can efficiently evaluate and automatically differentiate at arbitrary test locations. To this end, we now examine the direct approach to conditioning draws of  $f \sim \mathcal{GP}(\mu, k)$ .

### 3.2 Pathwise Conditioning

Examining the pathwise update given by Theorem 1, it is natural to suspect that an analogous statement holds for Gaussian processes. A quick check confirms this hypothesis.

**Corollary 4** *For a Gaussian process  $f \sim \mathcal{GP}(\mu, k)$  with marginal  $\mathbf{f}_n = f(\mathbf{X}_n)$ , the process conditioned on  $\mathbf{f}_n = \mathbf{y}$  may be expressed as*

$$\underbrace{(f \mid \mathbf{y})(\cdot)}_{\text{conditional}} \stackrel{\text{d}}{=} \underbrace{f(\cdot)}_{\text{prior}} + \underbrace{k(\cdot, \mathbf{X}_n) \mathbf{K}_{n,n}^{-1}(\mathbf{y} - \mathbf{f}_n)}_{\text{update}}. \quad (16)$$

**Proof** Follows by applying Theorem 1 to an arbitrary set of locations. ■

Figure 2 acts a visual guide to Corollary 4. From left to right, we begin by generating a realization of  $f \sim \mathcal{GP}(\mu, k)$  using methods that will soon be introduced in Section 4. Having obtained a sample path, we then use the pathwise update (16) to define a function  $k(\cdot, \mathbf{X}_n) \mathbf{K}_{n,n}^{-1}(\mathbf{y} - \mathbf{f}_n)$  to account for the residual  $\mathbf{y} - \mathbf{f}_n$ . Adding these two functions together produces a draw from a GP posterior, the behavior of which is shown on the right. Whereas



distributionally conditioning on  $\mathbf{f}_n = \mathbf{y}$  in (15) tells us how the GP’s statistic properties change, pathwise conditioning (16) tells us what happens to individual sample paths. This paradigm shift echoes the running theme: Gaussian (process) conditionals can be directly viewed in terms of random variables. The power of Corollary 4 is that it impacts *how* we think about Gaussian process posteriors and, therefore, *what* we do with them.

Having said this, there are several hurdles that we must overcome in order to use the pathwise update (16) in the real world. First, we are typically unable to practically sample functions  $f \sim \mathcal{GP}(\mu, k)$  from (non-degenerate) Gaussian process priors exactly. A Gaussian process can generally be written as a linear combination of elementary *basis functions*. When the requisite number of basis functions is infinite, however, evaluating this linear combination is usually impossible. In Section 4, we will therefore investigate different ways of approximating  $f(\cdot)$  using a finite number of operations.

Second, we incur  $\mathcal{O}(n^3)$  time complexity when naïvely carrying out (16), due to the need to solve the linear system of equations  $\mathbf{K}_{n,n}\mathbf{v} = \mathbf{y} - \mathbf{f}_n$  for a vector  $\mathbf{v} \in \mathbb{R}^n$  such that

$$(f \mid \mathbf{y})(\cdot) \stackrel{\text{d}}{=} f(\cdot) + \underbrace{\sum_{i=1}^n v_i k(\cdot, \mathbf{x}_i)}_{n\text{-dimensional basis}}. \quad (17)$$

Here, we have re-expressed the matrix-vector product in (16) as an expansion with respect to the canonical basis functions  $k(\cdot, \mathbf{x}_i)$  centered at training locations  $\mathbf{x}_i \in \mathbf{X}_n$ . For large training sets  $(\mathbf{x}_i, y_i)_{i=1}^n$ , direct application of (16) may prove prohibitively expensive. By the same token, the stated pathwise update does not hold when outcomes  $\mathbf{y}$  are not defined as realizations of process values  $\mathbf{f}_n$ . In Section 5, we will consider various means of resolving these challenges and ones like them.

### 3.3 Historical remarks

Prior to continuing, we pause to reflect on the historical developments that have paved the way for this work. In a 2005 tribute to geostatistics pioneer Georges Matheron, Chilès and Lantuéjoul (2005) comment that

[Matheron’s update rule] is nowhere to be found in Matheron’s entire published works, as he merely regarded it as an immediate consequence of the orthogonality of the [conditional expectation] and the [residual process].

As if to echo this very sentiment, Doucet (2010) begins a much appreciated technical note on the subject of Theorem 1 with the remark

This note contains no original material and will never be submitted anywhere for publication. However it might be of interest to people working with [Gaussian processes] so I am making it publicly available.

The presiding opinion, therefore, seems to be that Matheron’s update rule is *too simple* to warrant extended study. Indeed, Theorem 1 is exceedingly straightforward to verify. As is often the case, however, this result is harder to discover if one is not already aware of its existence. This dilemma may help to explain why Matheron’s update rule is absent from

standard machine learning texts. By deriving this result from first principles in Section 2.3, we hope to encourage fellow researchers to explore the strengths (and weaknesses) of the pathwise viewpoint espoused here.

We are not the first to have realized the practical implications of pathwise conditioning for GPs. Corollary 4 is relatively well-known in geostatistics (Journel and Huijbregts, 1978; de Fouquet, 1994; Emery, 2007; Chilès and Delfiner, 2012). Similarly, Oliver (1996) discusses Matheron’s update rule for Gaussian likelihoods (Section 5.1). Along the same lines, closely related ideas were rediscovered in the 1990s with applications to astrophysics. In particular, Hoffman and Ribak (1991) propose the use of spectral approximations to stationary priors (Section 4.2) in conjunction with canonical pathwise updates (17).

Nevertheless, these formulae are seldom seen in machine learning. We hope to systematically organize these findings (along with our own) and communicate them to a general audience of theorists and practitioners alike. The following sections therefore catalog various notable approaches to representing Gaussian process priors and pathwise updates.

## 4. Sampling functions from Gaussian process priors

The pathwise representation of GP posteriors described in the Section 3.2 allows us to represent  $f \mid \mathbf{y}$  by transforming a draw of  $f \sim \mathcal{GP}(0, k)$ . When interpreted as a generative strategy, this approach to sampling can only be deemed *efficient* if the tasks of realizing the prior and performing the update both scale favorably in the total number of locations  $|\mathbf{X}| = |\mathbf{X}_n| + |\mathbf{X}_*|$ . Half of the battle is, therefore, to obtain faithful but affordable draws of  $f$ . Fortunately, GP priors often exhibit convenient mathematical properties not present in their posteriors, which can be utilized to sample them efficiently.

We focus on methods for generating random *functions* that we may evaluate at arbitrary locations  $\mathbf{x} \in \mathcal{X}$  in  $\mathcal{O}(1)$  time and whose marginal distributions approximate those of  $f \sim \mathcal{GP}(0, k)$ . Conceptually, techniques discussed throughout this section will approximate GP priors as random linear combinations of suitably chosen basis functions  $\boldsymbol{\phi} = (\phi_1, \dots, \phi_\ell)$ . Specifically, we will focus on *Bayesian linear models* with Gaussian random weights

$$\tilde{f}(\cdot) = \sum_{i=1}^{\ell} w_i \phi_i(\cdot) \quad \mathbf{w} \sim \mathcal{N}(\mathbf{0}, \boldsymbol{\Sigma}_{\mathbf{w}}), \quad (18)$$

where the covariance of weights  $\mathbf{w}$  will vary by case. Notice that, for any finite collection of points  $\mathbf{X} \subset \mathcal{X}$ , the random vector  $\tilde{\mathbf{f}} = \tilde{f}(\mathbf{X})$  follows the Gaussian distribution  $\mathcal{N}(\mathbf{0}, \boldsymbol{\Phi} \boldsymbol{\Sigma}_{\mathbf{w}} \boldsymbol{\Phi}^\top)$ , where  $\boldsymbol{\Phi} = \boldsymbol{\phi}(\mathbf{X})$  is a  $|\mathbf{X}| \times \ell$  matrix of features. By design then,  $\tilde{f}$  is a Gaussian process. Rasmussen and Williams (2006) refer to (18) as the *weight-space* view of GPs.

From this perspective, the task of efficiently sampling the prior  $\tilde{f}$  reduces to one of generating random weights  $\mathbf{w}$ . In practice,  $\boldsymbol{\Sigma}_{\mathbf{w}}$  is typically diagonal, thereby enabling us to sample  $\tilde{f}$  in  $\mathcal{O}(\ell)$  time. We stress that, for any draw of  $\mathbf{w}$ , the corresponding realization of  $\tilde{f}$  is simply a deterministic function. In particular, we incur  $\mathcal{O}(1)$  cost for evaluating  $\tilde{f}(\mathbf{x})$  and may readily differentiate this term with respect to  $\mathbf{x}$  (or other parameters of interest).

Below, we review popular strategies for obtaining Bayesian linear models such that  $\tilde{f} \stackrel{\text{d}}{\approx} f$ . Our presentation is intended to communicate different angles for attacking this problem and is by no means exhaustive. To set the scene for these approaches, we begin by recounting some properties of the gold standard: location-scale methods.

### 4.1 Location-scale transformations

Location-scale methods (1) are the most widely used approach for generating Gaussian random vectors. These generative strategies are *exact* (up to machine precision). Given locations  $\mathbf{X}$ , we may simulate  $\mathbf{f} = f(\mathbf{X})$  in location-scale fashion

$$\mathbf{f}(\mathbf{X}) \stackrel{d}{=} \mathbf{K}^{1/2} \boldsymbol{\zeta} \quad \boldsymbol{\zeta} \sim \mathcal{N}(\mathbf{0}, \mathbf{I}) \quad (19)$$

by multiplying a square root covariance matrix  $\mathbf{K}^{1/2}$  by a standard normal vector  $\boldsymbol{\zeta}$ .

While (19) rightfully stands as the method of choice for many problems, it is not without shortcoming. Chief among these issues is the fact that algorithms for obtaining a matrix square root of  $\mathbf{K}$  scale cubically in  $|\mathbf{X}|$ . In most cases, this limits the use of location-scale approaches to cases where the length of the desired Gaussian random vector is manageable (up to several thousand). This overhead can be interpreted to mean that we incur  $\mathcal{O}(i^2)$  cost for realizing the  $i$ -th element of  $\mathbf{f}$ , which leads us to our second issue: reusing a draw of  $\mathbf{f}_n$  to efficiently generate the remainder of  $\mathbf{f} = \mathbf{f}_n \oplus \mathbf{f}_*$  requires us to sample from the conditional distribution

$$\mathbf{f}_* \mid \mathbf{f}_n \sim \mathcal{N}(\boldsymbol{\mu}_* + \mathbf{K}_{*,n} \mathbf{K}_{n,n}^{-1} (\mathbf{f}_n - \boldsymbol{\mu}_n), \mathbf{K}_{*,*} - \mathbf{K}_{*,n} \mathbf{K}_{n,n}^{-1} \mathbf{K}_{n,*}). \quad (20)$$

Despite matching asymptotic costs, iterative approaches to sampling  $\mathbf{f}$  are substantially slower than simultaneous ones. In applied settings, however, test locations  $\mathbf{X}_*$  are often determined adaptively, forcing location-scale-based methods for generating  $\mathbf{f}$  to repeatedly compute (20). Further refining this predicament, we arrive at a final challenge: pathwise derivatives.

Differentiation is a linear operation. The gradient of a Gaussian process  $f$  with respect to a location  $\mathbf{x}$  is, therefore, another Gaussian process  $f'$ . By construction, these GPs are correlated. Using gradient information to maneuver along a sample path—for example, to identify its extrema—therefore requires us to re-condition both processes on the realized values of  $f(\mathbf{x})$  and  $f'(\mathbf{x})$  at each successive step of gradient descent.

Prior to continuing, it is worth noting that the limitations of location-scale methods can be avoided in certain cases. In particular, the otherwise cubic costs for computing a square root in (19) can be dramatically reduced by exploiting structural assumptions regarding covariance matrices  $\mathbf{K}$ . Well-known examples of structured matrices include banded and sparse ones in the context of one-dimensional Gaussian processes and Gauss–Markov random fields (Rue and Held, 2005; Durrande et al., 2019; Loper et al., 2020), block-Toeplitz Toeplitz-block ones when evaluating stationary product kernels on regularly-spaced grids  $\mathbf{X} \subset \mathcal{X}$  (Zimmerman, 1989; Wood and Chan, 1994; Dietrich and Newsam, 1997), and kernel-interpolation-based ones (Wilson and Nickisch, 2015; Pleiss et al., 2018). When the task at hand permits their usage, these methods are highly effective.

The following sections survey different approaches to overcoming the challenges put forth above by approximating Gaussian process priors as finite-dimensional Bayesian linear models.

### 4.2 Stationary covariances

Stationary covariance functions  $k(\mathbf{x}, \mathbf{x}') = k(\mathbf{x} - \mathbf{x}')$ , such as the Matérn family’s limiting squared exponential kernel, give rise to a significant portion of GP priors in use today. For

centered priors  $f \sim \mathcal{GP}(0, k)$ , stationarity encodes the belief that the relationship between process values  $f(\mathbf{x}_i)$  and  $f(\mathbf{x}_j)$  is solely determined by the difference  $\mathbf{x}_i - \mathbf{x}_j$  between locations  $\mathbf{x}_i$  and  $\mathbf{x}_j$ . Simple but expressive, stationarity is the go-to modeling assumption in many applied settings.

These kernels exhibit a variety of special properties that greatly facilitate the construction of efficient, approximate priors. Here, we restrict attention to kernels admitting a spectral density  $\rho$ , and focus on the class of estimators formed by discretizing the spectral representation of  $k$

$$k(\mathbf{x} - \mathbf{x}') = \int_{\mathbb{R}^d} e^{2\pi i \boldsymbol{\omega}^\top (\mathbf{x} - \mathbf{x}')} \rho(\boldsymbol{\omega}) d\boldsymbol{\omega} \quad \rho(\boldsymbol{\omega}) = \int_{\mathbb{R}^d} e^{-2\pi i \boldsymbol{\omega}^\top \mathbf{x}} k(\mathbf{x}) d\mathbf{x}. \quad (21)$$

By the *kernel trick* (Schölkopf and Smola, 2001), a kernel  $k$  can be written as the inner product in a corresponding reproducing kernel Hilbert space (RKHS)  $\mathcal{H}_k$  equipped with a feature map  $\varphi : \mathcal{X} \rightarrow \mathcal{H}_k$ . In many cases, this inner product can be approximated by

$$k(\mathbf{x}, \mathbf{x}') = \langle \varphi(\mathbf{x}), \varphi(\mathbf{x}') \rangle_{\mathcal{H}_k} \approx \boldsymbol{\phi}(\mathbf{x})^\top \overline{\boldsymbol{\phi}(\mathbf{x}')}, \quad (22)$$

where  $\boldsymbol{\phi} : \mathcal{X} \rightarrow \mathbb{C}^\ell$  is some finite-dimensional feature map and  $\overline{\boldsymbol{\phi}(\mathbf{x}'})$  denotes the complex conjugate. Based on this idea, the method of *random Fourier features* (Rahimi and Recht, 2008) constructs a Monte Carlo estimate to a stationary kernel by representing the right-hand side of (22) with  $\ell$  complex exponential basis functions  $\phi_j(\mathbf{x}) = \ell^{-1/2} \exp(2\pi i \boldsymbol{\omega}_j^\top \mathbf{x})$ , whose parameters  $\boldsymbol{\omega}_j$  are sampled proportional to the corresponding spectral density  $\rho(\boldsymbol{\omega}_j)$ .<sup>2</sup>

Given an  $\ell$ -dimensional basis  $\boldsymbol{\phi} = (\phi_1, \dots, \phi_\ell)$ , we may now proceed to approximate the true prior according to the Bayesian linear model

$$\tilde{f}(\cdot) = \sum_{i=1}^{\ell} w_i \phi_i(\cdot) \quad w_i \sim \mathcal{N}(0, 1). \quad (23)$$

Under this approximation,  $\tilde{f}$  is a random function satisfying  $\tilde{\mathbf{f}}_n \sim \mathcal{N}(\mathbf{0}, \boldsymbol{\Phi}_n \boldsymbol{\Phi}_n^\top)$ , where  $\boldsymbol{\Phi}_n = \boldsymbol{\phi}(\mathbf{X}_n)$  is an  $n \times \ell$  matrix of features. Per the beginning of this section, then,  $\tilde{f}$  is a Gaussian process whose covariance approximates that of  $f$ .

The random Fourier feature approach is particularly appealing since its position as a Monte Carlo estimator implies that the error introduced by the  $\ell$ -dimensional basis  $\boldsymbol{\phi}$  decays at the *dimension-free* rate  $\ell^{-1/2}$  (Sutherland and Schneider, 2015). This property enables us to balance accuracy and cost by choosing  $\ell$  to suite the task at hand.

### 4.3 Karhunen–Loève expansions

While exploitation of stationarity is arguably the most common route when constructing approximate priors, it is neither unique nor optimal. A powerful alternative is to utilize the *Karhunen–Loève expansion* of a Gaussian process prior (Castro et al., 1986; Fukunaga, 2013).

We begin by considering the family of  $\ell$ -dimensional Bayesian linear models  $\tilde{f}(\cdot) = \boldsymbol{\phi}(\cdot)^\top \mathbf{w}$  consisting of orthonormal basis functions  $\phi_i : \mathcal{X} \rightarrow \mathbb{R}$  on a compact space  $\mathcal{X}$ . Following

2. Using elementary trigonometric identities, we may also derive a related family of basis functions  $\phi : \mathcal{X} \rightarrow \mathbb{R}^\ell$  with  $\phi_j(\mathbf{x}) = \sqrt{2/\ell} \cos(2\pi \boldsymbol{\omega}_j^\top \mathbf{x} + \tau_j)$ , where  $\tau_j \sim \mathcal{U}(0, 2\pi)$ .

standard theory (Fukunaga, 2013), the *optimal*  $\tilde{f}$  for approximating a Gaussian process  $f$  (in the sense of minimizing mean square error) is found by truncating its Karhunen–Loève expansion

$$f(\cdot) = \sum_{i=1}^{\infty} w_i \phi_i(\cdot) \quad w_i \sim \mathcal{N}(0, \lambda_i), \quad (24)$$

where  $\phi_i$  and  $\lambda_i$  are, respectively, the  $i$ -th eigenfunction and eigenvalue of the covariance operator  $\psi \mapsto \int_{\mathcal{X}} \psi(\mathbf{x}) k(\mathbf{x}, \cdot) d\mathbf{x}$ , written in decreasing order of  $\lambda_i$ .<sup>3</sup> Truncated versions of these expansions are used as both bases for constructing optimal approximate GPs (Zhu et al., 1997; Solin and Särkkä, 2020) and modeling tools in their own right (Krainski et al., 2018). Depending on the case, eigenfunctions  $\phi_i$  are either derived from first principles (Krainski et al., 2018) or obtained by numerical methods (Lindgren et al., 2011; Lord et al., 2014; Solin and Kok, 2019).

In addition to being optimal, Karhunen–Loève expansions are exceedingly general. Even when a covariance function  $k$  is non-stationary or the domain  $\mathcal{X}$  is non-Euclidean—such as when Gaussian processes are used to represent functions on manifolds (Borovitskiy et al., 2020) and graphs (Borovitskiy et al., 2021)—the Karhunen–Loève expansion often exists.

Widespread use of truncated eigensystems is largely impeded by their frequent lack of convenient, analytic forms. This issue is compounded by the fact that efficient, numerical methods for obtaining (24) typically require us to manipulate bespoke mathematical properties of specific kernels. These properties are often closely related to the differential-equation-based perspectives of Gaussian processes introduced in the following section.

#### 4.4 Stochastic partial differential equations

Many Gaussian process priors, such as the Matérn family, can be expressed as solutions of *stochastic partial differential equations* (SPDEs). SPDEs are common in fields such as physics, where they describe natural phenomena (such as diffusion and heat transfer); many of which share a deep connection with the squared exponential kernel (Grigoryan, 2009). Additionally, SPDEs are often the starting point when designing non-stationary GP priors (Krainski et al., 2018). Below, we detail how the *Galerkin finite element method* (Evans, 2010; Lindgren et al., 2011; Lord et al., 2014) can be used to construct Bayesian linear models that approximate GP priors capable of being represented as SPDEs.

Suppose a Gaussian process  $f \sim \mathcal{GP}(0, k)$  satisfies  $\mathcal{L}f = \mathcal{W}$ , where  $\mathcal{L}$  is a linear differential operator and  $\mathcal{W}$  is a Gaussian white noise process (Lifshits, 2012). Here, we demonstrate how to derive a Gaussian process  $\tilde{f}$  that approximately satisfies this SPDE. To begin, we express  $\mathcal{L}f = \mathcal{W}$  in its weak form<sup>4</sup>

$$\int_{\mathcal{X}} (\mathcal{L}f)(\mathbf{x}) g(\mathbf{x}) d\mathbf{x} = \int_{\mathcal{X}} g(\mathbf{x}) d\mathcal{W}(\mathbf{x}), \quad (25)$$

where  $g$  is an arbitrary element of an appropriate class of test functions. Next, we proceed by approximating both the desired solution  $f$  and the test function  $g$  with respect to a

3. These eigenvalues are well-ordered and countable as consequence of the compactness of  $\mathcal{X}$ .

4. One typically integrates  $(\mathcal{L}f)(\mathbf{x}) g(\mathbf{x})$  by parts, either by necessity or due to affordances of the basis  $\phi_i$ . We suppress this to ease notation.

finite-dimensional basis as  $\tilde{f}(\cdot) = \sum_{i=1}^{\ell} w_i \phi_i(\cdot)$  and  $\tilde{g}(\cdot) = \sum_{j=1}^{\ell} v_j \phi_j(\cdot)$ . Substituting these terms into (25) and differentiating both sides with respect to the coefficients of  $\tilde{g}$ , we obtain the following expression for each  $j = 1, \dots, \ell$

$$\sum_{i=1}^{\ell} w_i \underbrace{\int_{\mathcal{X}} (\mathcal{L}\phi_i)(\mathbf{x}) \phi_j(\mathbf{x}) d\mathbf{x}}_{A_{ij}} = \underbrace{\int_{\mathcal{X}} \phi_j(\mathbf{x}) d\mathcal{W}(\mathbf{x})}_{b_j}. \quad (26)$$

Defining  $\mathbf{M} = \text{Cov}(\mathbf{b})$ , where  $\text{Cov}(b_i, b_j) = \langle \phi_i, \phi_j \rangle$  coincides with the finite-element mass matrix, allows us to rearrange this system of random linear equations in matrix-vector form by writing  $\mathbf{A}\mathbf{w} = \mathbf{b}$ . The basis coefficients of the random function  $\tilde{f}$  are, therefore, distributed as  $\mathbf{w} \sim \mathcal{N}(\mathbf{0}, \mathbf{A}^{-1}\mathbf{M}\mathbf{A}^{-\top})$ . As in the previous sections,  $\tilde{f}$  can be seen as the weight-space view of a corresponding Gaussian process.

A popular choice is to employ compactly supported basis functions  $\phi_i$  (Lindgren et al., 2011). The matrices  $\mathbf{A}$  and  $\mathbf{M}$  are then sparse, and the resulting linear systems can be solved efficiently. For example, the family of piecewise linear basis functions is a simple but effective choice for second order differential operators  $\mathcal{L}$  (Evans, 2010; Lord et al., 2014).<sup>5</sup>

## 4.5 Discussion

This section has focused on identifying finite-dimensional bases with which to construct Bayesian linear models  $\tilde{f}(\cdot) = \phi(\cdot)^\top \mathbf{w}$ . These model can be seen as *weight-space* interpretations (Rasmussen and Williams, 2006) of corresponding Gaussian process priors  $\tilde{f} \sim \mathcal{GP}(0, \tilde{k})$  with covariance functions  $\tilde{k}(\mathbf{x}, \mathbf{x}') = \phi(\mathbf{x})^\top \Sigma_{\mathbf{w}} \phi(\mathbf{x}')$ . Since  $\mathbf{w}$  and  $\tilde{\mathbf{f}}_n = \Phi_n \mathbf{w}$  are jointly normal, Theorem 1 implies that we may enforce the condition  $\tilde{\mathbf{f}}_n = \mathbf{y}$  by writing<sup>6</sup>

$$\phi(\cdot)^\top (\mathbf{w} \mid \mathbf{y}) \stackrel{d}{=} \phi(\cdot)^\top \left( \mathbf{w} + \Phi_n^\top (\Phi_n \Phi_n^\top)^{-1} (\mathbf{y} - \Phi_n \mathbf{w}) \right). \quad (27)$$

This result encourages us to approximate posteriors in much the same way as we have priors. After all, if we have chosen a basis  $\phi$  that encodes our prior knowledge for  $f$  (such as how smooth we believe this function to be), then it is reasonable to think that  $\phi$  will further enable us to efficiently approximate  $f \mid \mathbf{y}$ . To the extent that this approach may seem like the natural evolution of ideas discussed in this section, we argue for the benefits of *decoupling* the representation of the prior from that of the data.

The trouble with using a finite set of homogeneous basis functions  $\phi = (\phi_1, \dots, \phi_\ell)$  to represent both the prior and the data is that these two tasks focus on different things. To accurately approximate a prior is to faithfully describe a random function  $f$  on a domain  $\mathcal{X}$ . Consequently, parsimonious approximations  $\tilde{f}$  employ global basis functions that vary non-trivially everywhere on  $\mathcal{X}$ . This is largely why, e.g., Fourier features are an attractive choice for approximating stationary priors. But what of the data?

Conditioning on observations  $\mathbf{y}$  requires us to convey how our understanding of  $f$  has changed. In most cases, we choose priors (and likelihoods) that reflect the belief that an

5. A second order differential operator gives rise to a first-order bilinear form when integrated by parts, which matches with piecewise linear basis functions which are once differentiable almost everywhere. For higher-order operators, a piecewise polynomial basis may be used instead.

6. Practical variants of (27) avoid inverting  $\Phi_n \Phi_n^\top$  by employing, e.g., Gaussian likelihoods (Section 5.1).

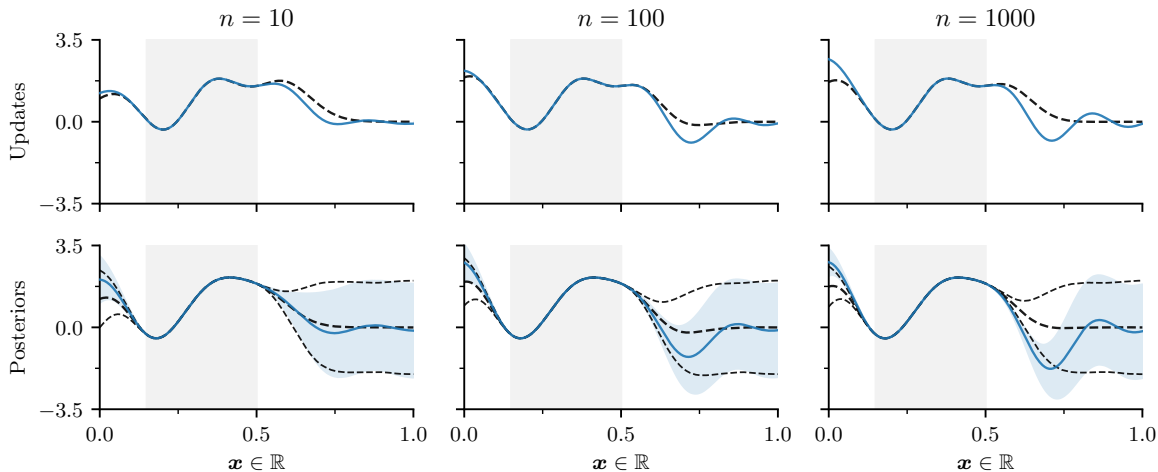


Figure 3: Overview of variance starvation when conditioning on  $n \in \{10, 100, 1000\}$  observations of the form  $y_i \sim \mathcal{N}(f_i, 10^{-5})$  located within the gray shaded region. *Top*: Comparison of pathwise updates to a single draw from an approximate prior  $\tilde{f}(\cdot) = \phi(\cdot)^\top \mathbf{w}$ , constructed using  $\ell = 1000$  Fourier features  $\phi$ . Updates defined using the same Fourier basis  $\phi(\cdot)$  and the canonical basis functions  $k(\cdot, \mathbf{X})$  are shown in blue and dashed-black, respectively. *Bottom*: Mean and two standard deviations of the empirical posteriors formed by applying the aforementioned updates to  $10^5$  draws from the approximate prior.

observation  $y_i$  only informs us about the process  $f$  in the immediate vicinity of a point  $\mathbf{x}_i$ . Updating  $f$  to account for  $\mathbf{y}$ , therefore, typically focuses on process values corresponding to specific regions of  $\mathcal{X}$ . Rather than global basis functions, the data is best characterized by local ones that have near-zero values outside of the aforementioned regions. Not coincidentally, the canonical basis functions  $k(\cdot, \mathbf{x})$  fit this description perfectly when the chosen prior implies that  $y_i$  is only locally informative.

A key property of pathwise conditioning is that it not only provides us with a natural decomposition of GP posteriors—as sums of prior random variables and data-driven updates—but enables us to represent these terms in separate bases. Similar ideas can be found in recent works that explore alternative decompositions of Gaussian processes, such as separation of mean and covariance functions (Cheng and Boots, 2017; Salimbeni et al., 2018) or decoupling of RKHS subspaces and their orthogonal complements (Shi et al., 2020). Unlike these works, however, we stress decoupling in the sense of using different classes of basis functions to represent different aspects of GP posteriors. While this type of decoupling is not unique to pathwise approaches (Lázaro-Gredilla and Figueiras-Vidal, 2009; Hensman et al., 2017), they drastically simplify the process by eliminating the need to analytically solve for sufficient statistics.

This line of reasoning also helps to explain why finite-dimensional GPs constructed from homogeneous basis functions often produce poorly-calibrated posteriors. For now, we restrict our attention to the issue of *variance starvation* (Wang et al., 2018; Mutny and Krause, 2018; Calandriello et al., 2019) and return this topic in Section 5.5. Figure 3 demonstrates what happens as the number of observations  $n = |\mathbf{y}|$  approaches the number of random Fourier features  $\ell = 1000$  used to approximate a squared exponential kernel. In general,

the approximate posteriors produce extrapolations which become increasingly erratic. Note that the rate at which these defects materialize depends upon the choice of kernel and likelihood. In the figure, posteriors yielded by pathwise updates in canonical and Fourier bases (all other things being held equal) diverge as the number of observations  $n$  approaches the number of random Fourier features  $\ell$ . This pattern emerges because the Fourier basis is better at describing stationary priors than non-stationary posteriors. Fourier features excel at capturing the global properties of the prior, but struggle to portray the localized effects of the data.

Of course, different types of data impose different kinds of conditions on the process  $f$ . We now examine various pathwise updates that enforce prominent types of conditions.

## 5. Conditioning via pathwise updates

Building off of the foundation prepared in Section 3, we now adapt Corollary 4 to accommodate different types of conditions and computational budgets. Throughout this section, we use  $\gamma$  to denote the random variable realized by observations  $\mathbf{y}$  under the chosen likelihood.

### 5.1 Gaussian updates

Corollary 4 treats observations  $\mathbf{y}$  as a realization of process values  $\mathbf{f}_n = f(\mathbf{X}_n)$ . Hence, the conditions it imposes manifest as the equality constraint  $\mathbf{f}_n = \mathbf{y}$ . In the real world, however, we seldom observe  $\mathbf{f}_n$  directly. To account for this nuance, an observation  $y$  is modeled by a *likelihood*  $p(y \mid f(\mathbf{x}))$ . Viewed from this perspective, the equality constraint  $\mathbf{f}_n = \mathbf{y}$  correspond to the limit where  $p$  contracts to a point mass. Seeing as  $y$  usually fails to fully disambiguate the true value of  $f(\mathbf{x})$ , we typically employ likelihoods that induce weaker conditions than strict equalities.

For regression problems, the most common choice is to employ a Gaussian likelihood  $p(y \mid f(\mathbf{x})) = \mathcal{N}(y \mid f(\mathbf{x}), \sigma^2)$ , the log of which penalizes the squared Euclidean distance of  $f(\mathbf{x})$  from  $y$ . Under the corresponding observation model  $\gamma = \mathbf{f}_n + \varepsilon$  with  $\varepsilon \sim \mathcal{N}(\mathbf{0}, \sigma^2 \mathbf{I})$ ,  $f$  and  $\mathbf{y}$  are jointly Gaussian. By Corollary 4 then, we may condition  $f$  on  $\gamma = \mathbf{y}$  by writing

$$(f \mid \gamma = \mathbf{y})(\cdot) \stackrel{\text{d}}{=} f(\cdot) + k(\cdot, \mathbf{X})(\mathbf{K}_{n,n} + \sigma^2 \mathbf{I})^{-1}(\mathbf{y} - \mathbf{f}_n - \varepsilon). \quad (28)$$

Rather than exactly passing through observations  $\mathbf{y}$ , the conditioned path  $f \mid \mathbf{y}$  now smoothly interpolates between them. In cases where  $\gamma$  is not a Gaussian random variable, additional tools are needed.

### 5.2 Non-Gaussian updates

In the general setting, where the random variable  $\gamma$  is arbitrarily distributed under the chosen likelihood,  $\gamma$  relates to process values  $\mathbf{f}$  by way of the non-conjugate prior

$$p(\gamma, \mathbf{f}) = p(\gamma \mid g^{-1}(\mathbf{f})) \mathcal{N}(\mathbf{f} \mid \boldsymbol{\mu}, \mathbf{K}), \quad (29)$$

where the *link function*  $g : \mathcal{Y} \rightarrow \mathbb{R}$  maps from the space of predictions  $\mathcal{Y} \subset \mathbb{R}$  to the range of  $f$ . For binary classification problems, popular choices for  $g : [0, 1] \rightarrow \mathbb{R}$  include logit and probit functions (Rasmussen and Williams, 2006). The left column of Figure 4 illustrates this scenario using methods described below.



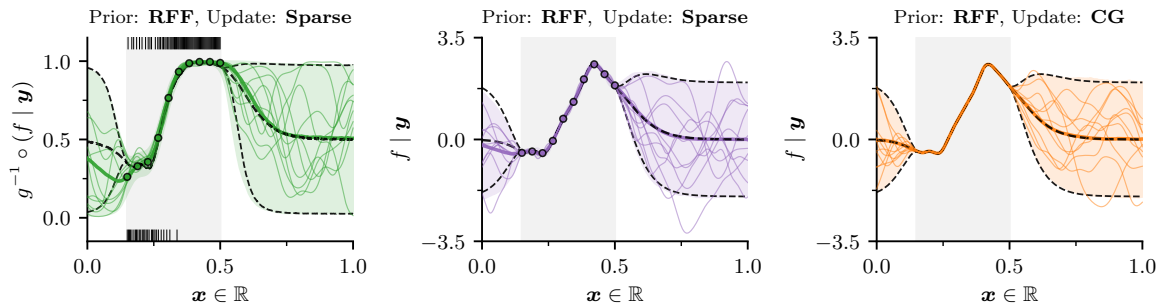


Figure 4: Visual comparison of different pathwise updates. *Left and middle:* Variational inference is used to learn sparse updates at  $m = 10$  inducing locations  $\mathbf{Z}$  (circles). *Right:* preconditioned conjugate gradients is used to iteratively solve for Gaussian updates. In all cases, 1000 observations  $\mathbf{y}$  are evenly spaced in the shaded region. Dashed lines denote mean and two standard deviations of ground truth posteriors, colored regions and thicker lines denote those of empirical ones. Middle and right plots illustrate regression with a Gaussian likelihood  $\mathcal{N}(y_i | f_i, 10^{-3})$ . The left plot shows binary classification with a Bernoulli likelihood and probit link function  $g$ ; every tenth label is shown as a small, vertical bar.

Even under a non-conjugate prior (29), the conditional expectation  $\mathbb{E}(f | \gamma)$  and the residual  $f - \mathbb{E}(f | \gamma)$  it induces are uncorrelated (see Section 2.3). Since  $p(\mathbf{f}, \gamma)$  may not be Gaussian, however, it no longer follows that this lack of correlation implies independence—hence, the pathwise update (16) may not hold.

Exact Bayesian inference and prediction are typically intractable when dealing with non-conjugate priors. Strategies for circumventing this issue generally approximate the true posterior by introducing an auxiliary random variable  $\mathbf{u} \sim q(\mathbf{u})$  such that  $f | \mathbf{u}$  resembles  $f | \mathbf{y}$  according to a chosen measure of similarity (Nickisch and Rasmussen, 2008; Hensman et al., 2015). For practical reasons,  $\mathbf{u}$  is typically assumed to be jointly Gaussian with  $\mathbf{f}$ .<sup>7</sup> Consequently, non-conjugate priors  $p(\mathbf{f}, \gamma)$  are replaced by conjugate ones  $p(\mathbf{f}, \mathbf{u})$  to aid in the construction of approximate posteriors, whereupon Matheron’s update rule holds once more. The following section explores these *sparse* approximations in greater detail.

### 5.3 Sparse updates

Approximations to GP posteriors frequently revolve around conditioning a process  $f$  on a random variable  $\mathbf{u} = (u_1, \dots, u_m) \in \mathbb{R}^m$ . Per the previous section, this may be because the outcome variable  $\gamma$  is non-Gaussian (Nickisch and Rasmussen, 2008; Titsias and Lawrence, 2010; Hensman et al., 2015). Alternatively, the  $\mathcal{O}(n^3)$  cost for directly conditioning on all  $n = |\mathbf{y}|$  observations may be prohibitive (Titsias, 2009a; Hensman et al., 2013). In these cases and more, we would like to infer a distribution  $q(\mathbf{u})$  such that  $f | \mathbf{u}$  explains the data. Defining (approximate) posteriors in this way not only avoids potential issues arising from non-Gaussianity of  $\gamma$ , but associates the computational cost of conditioning with  $\mathbf{u}$ . As discussed below, this leads to pathwise updates that run in  $\mathcal{O}(m^3)$  time.

Comprehensive treatment of different approaches to learning *inducing distributions*  $q(\mathbf{u})$  is beyond the scope of this work. In general, however, these procedures operate by finding

7. Note that, in the special case where  $p(\mathbf{f}, \gamma)$  is Gaussian, the optimal  $q$  is also Gaussian (Titsias, 2009b).

an approximate posterior  $q(\mathbf{f}, \mathbf{u})$  within a tractable family of approximating distributions  $\mathcal{Q}$ . For reasons that will soon become clear, this family of distributions typically includes an additional set of parameters  $\mathbf{Z}$ , which help to define the joint distribution  $p(\mathbf{f}, \mathbf{u})$ . To help streamline presentation, we focus on the simplest and most widely used abstraction for inducing variables  $\mathbf{u}$ : namely, *pseudo-data*.

The noise-free pseudo-data framework (Snelson and Ghahramani, 2006; Quiñonero-Candela et al., 2007; Titsias, 2009a) treats each draw of a random vector  $\mathbf{u} \sim q(\mathbf{u})$  as a realization of process values  $\mathbf{f}_m = f(\mathbf{Z})$  at a corresponding set of tunable locations  $\mathbf{Z} \in \mathcal{X}^m$ . This paradigm gets its name from the intuition that the (random) collection of pseudo-data  $(\mathbf{z}_j, u_j)_{j=1}^m$  mimics the effect of a noise-free data set  $(\mathbf{x}_i, f_i)_{i=1}^n$  on  $f$ . By construction,  $\mathbf{u}$  is jointly Gaussian with  $f$ .<sup>8</sup> Appealing to Corollary 4, we define the *sparse pathwise update* as

$$(f | \mathbf{u})(\cdot) \stackrel{\text{d}}{=} f(\cdot) + \underbrace{\sum_{i=1}^m v_i k(\cdot, \mathbf{z}_i)}_{m\text{-dimensional basis}}, \quad (30)$$

where  $\mathbf{v} = \mathbf{K}_{m,m}^{-1}(\mathbf{u} - \mathbf{f}_m)$ . This formula is identical to the one given by Corollary 4, save for the fact that we now sample  $\mathbf{u} \sim q(\mathbf{u})$  and solve for a linear system involving the  $m \times m$  covariance matrix  $\mathbf{K}_{m,m} = k(\mathbf{Z}, \mathbf{Z})$  at  $\mathcal{O}(m^3)$  cost. The middle column of Figure 4 illustrates the sparse update induced by Gaussian  $\mathbf{u} \sim \mathcal{N}(\boldsymbol{\mu}_u, \boldsymbol{\Sigma}_u)$  with learned moments  $\boldsymbol{\mu}_u$  and  $\boldsymbol{\Sigma}_u$ .

Just as we can imitate process values  $\mathbf{f}_n$ , we can also emulate (Gaussian) observations  $\mathbf{y}$ . This intuition leads to the Gaussian pseudo-data family of inducing distributions, whose moments

$$\boldsymbol{\mu}_u = \mathbf{K}_{m,m}(\mathbf{K}_{m,m} + \boldsymbol{\Lambda})^{-1} \tilde{\mathbf{y}} \quad \boldsymbol{\Sigma}_u = (\mathbf{K}_{m,m}^{-1} + \boldsymbol{\Lambda})^{-1} \quad (31)$$

are parameterized by *pseudo-observations*  $\tilde{\mathbf{y}} \in \mathbb{R}^m$  and *pseudo-noise*  $\tilde{\boldsymbol{\sigma}} \in \mathbb{R}_+^m$ , where  $\boldsymbol{\Lambda} = \text{diag}(\tilde{\boldsymbol{\sigma}}^2)$ . This choice of parameterization is motivated by the observation that, given  $n \leq m$  Gaussian random variables  $\boldsymbol{\gamma} \sim \mathcal{N}(\mathbf{f}_n, \sigma^2 \mathbf{I})$ , the family of distributions it generates contains the optimal  $q$  despite housing only  $\mathcal{O}(m)$  free terms (Seeger, 1999; Oppen and Archambeau, 2009).<sup>9</sup> Using the Gaussian pathwise update (28), we may express  $\mathbf{u}$  itself as

$$\mathbf{u} \stackrel{\text{d}}{=} \mathbf{f}_m + \mathbf{K}_{m,m}(\mathbf{K}_{m,m} + \boldsymbol{\Lambda})^{-1}(\tilde{\mathbf{y}} - \mathbf{f}_m - \tilde{\boldsymbol{\epsilon}}) \quad \tilde{\boldsymbol{\epsilon}} \sim \mathcal{N}(\mathbf{0}, \boldsymbol{\Lambda}). \quad (32)$$

Here, despite the fact that  $\mathbf{f}_m$  and  $\tilde{\boldsymbol{\epsilon}}$  generate  $\mathbf{u}$ , it remains the case that  $\text{Cov}(\mathbf{f}_m + \tilde{\boldsymbol{\epsilon}}, \mathbf{u}) = \mathbf{0}$ . Substituting this expression into (30) and simplifying gives the pathwise update<sup>10</sup>

$$(f | \mathbf{u})(\cdot) \stackrel{\text{d}}{=} f(\cdot) + k(\cdot, \mathbf{Z})(\mathbf{K}_{m,m} + \boldsymbol{\Lambda})^{-1}(\tilde{\mathbf{y}} - \mathbf{f}_m - \tilde{\boldsymbol{\epsilon}}). \quad (33)$$

Hence, while sampling  $\mathbf{u}$  is more complicated in the Gaussian pseudo-data case, the resulting pathwise update is straightforward. This family of inducing distributions is particularly advantageous in the large  $m$  setting, both because it contains only  $\mathcal{O}(m)$  free parameters and for reasons discussed in the following section.

8. This condition holds when  $\mathbf{u}$  relates to  $f$  via a linear map (Lázaro-Gredilla and Figueiras-Vidal, 2009).

9. We recover the true posterior by, e.g., taking  $(\tilde{y}_i, \tilde{\sigma}_i) = (y_i, \sigma)$  for all  $i \leq n$  and sending  $\tilde{\sigma}_i \rightarrow \infty$  otherwise.

10. This same line of reasoning leads to a *rank-1 pathwise update* for cases where conditions arrive online.

In rough analogy to methods discussed in Section 4, we may think of the sparse updates introduced here as using an  $m$ -dimensional basis  $k(\cdot, \mathbf{Z})$  to approximate functions defined in terms of the  $n$ -dimensional basis  $k(\cdot, \mathbf{X}_n)$ . In practice, this basis is often efficient because neighboring training locations give rise to similar basis functions. Kernel basis functions at appropriately chosen sets of  $m \ll n$  locations  $\mathbf{Z}$  exploit this redundancy to produce a sparser, more cost-efficient representation. Burt et al. (2020) study this problem in detail and derive bounds on the quality of variational approximations to GP posteriors as  $m \rightarrow n$ .

## 5.4 Iterative solvers

Throughout this section, we have focused on the high-level properties of pathwise updates in relation to various problem settings. We have said little, however, regarding the explicit means of executing such an update. In all cases discussed here, pathwise updates have amounted to solutions to system of linear equations. For example, the update originally featured in Corollary 4 solves the system  $\mathbf{K}_{n,n}\mathbf{v} = \mathbf{y} - \mathbf{f}_n$  for a vector of coefficients  $\mathbf{v}$ , which define how the same realization of  $f$  changes when subjected to the condition  $\mathbf{f}_n = \mathbf{y}$ . Given a reasonable number of conditions  $n$  (up to several thousand), we may obtain  $\mathbf{v}$  by first computing the Cholesky factor  $\mathbf{L}_{n,n} = \mathbf{K}_{n,n}^{1/2}$  and then solving for a pair of triangular systems  $\mathbf{L}_{n,n}\bar{\mathbf{v}} = \mathbf{u} - \mathbf{f}_n$  and  $\mathbf{L}_{n,n}^\top \mathbf{v} = \bar{\mathbf{v}}$ . For large  $n$ , however, the  $\mathcal{O}(n^3)$  time complexity for carrying out this recipe is typically prohibitive.

Rather than solving for coefficients  $\mathbf{v}$  directly, we may instead employ an *iterative solver* that constructs a sequence of estimates  $\mathbf{v}^{(1)}, \mathbf{v}^{(2)}, \dots$  to  $\mathbf{v}$ , such that  $\mathbf{v}^{(j)}$  converges to the true  $\mathbf{v}$  as  $j$  increases. Depending on the numerical properties of the linear system in question, it is possible (or even likely) that a high-quality estimate  $\mathbf{v}^{(j)}$  will be obtained after only  $j \ll n$  iterations. This line of reasoning features prominently in a number of recent works, where iterative solvers have been shown to be highly competitive for purposes of approximating GP posteriors (Pleiss et al., 2018; Gardner et al., 2018; Wang et al., 2019). The right column of Figure 4 visualizes an iterative solution to the Gaussian pathwise update (28) obtained using preconditioned conjugate gradients (Gardner et al., 2018).

In these cases, posterior sampling via pathwise conditioning enjoys an important advantage over distributional approaches: it allows us to solve for linear system of the form  $\mathbf{K}_{n,n}^{-1}\mathbf{v}$  rather than working with  $\mathbf{K}_{*,*|n}^{1/2}\boldsymbol{\zeta}$ . Whereas the former amounts to a standard solve, the latter often requires special considerations (Pleiss et al., 2020) and can be difficult to work with when typical square root decompositions prove impractical (Parker and Fox, 2012).

Lastly, we note that these techniques can be combined with sparse approximations for improved scaling in  $m$  and faster convergence of iterative solves. As a concrete example, we return to the Gaussian pseudo-data variational family (31). By construction, the corresponding pathwise update (33) closely resembles the original Gaussian update (28). In general, however, pseudo-noise variances  $\tilde{\sigma}_i^2$  are often significantly larger than the true noise variance  $\sigma^2$ . The resulting linear system  $(\mathbf{K}_{m,m} + \boldsymbol{\Lambda})^{-1}\mathbf{v}$  is, therefore, substantially better-conditioned than that of the exact alternative—implying that it can be solved in far fewer iterations.

## 5.5 Discussion

In Section 4.5, we discussed finite-dimensional approximations of Gaussian process posteriors. There, we explored how the globality of the prior reinforces the use of basis functions  $\phi_i : \mathcal{X} \rightarrow \mathbb{R}$  that inform us about  $f$  over the entire domain  $\mathcal{X}$ , while the localized effects of the data encourages the use of  $\phi_i$  that only tell us about  $f$  on subsets of  $\mathcal{X}$ . This conflict hinders our ability to efficiently represent both the prior and the data (i.e., the posterior) using a single class of basis functions. That discussion ended with a demonstration of what happens when  $\phi = (\phi_1, \dots, \phi_\ell)$  solely consists of global basis functions, specifically random Fourier features. Most works, however, have focused on the use of canonical basis functions  $k(\cdot, \mathbf{x})$ , which are typically local. This section, therefore, aims to fill in the gaps.

At the end of Section 4.5, we saw how trouble conveying the data in global bases led to approximate posteriors that were starved for variance (Figure 3). Writing the update rules—for a draw from an approximate prior  $\tilde{f}(\cdot) = \phi(\cdot)^\top \mathbf{w}$  subject to the condition  $\tilde{\mathbf{f}}_n = \mathbf{y}$ —in both unified and decoupled bases side-by-side helps to highlight their key differences

$$\underbrace{\tilde{f}(\cdot) + \phi(\cdot)^\top \Phi_n^\top (\Phi_n \Phi_n^\top)^{-1} (\mathbf{y} - \tilde{\mathbf{f}}_n)}_{\text{unified approximate posterior}} \quad \underbrace{\tilde{f}(\cdot) + k(\cdot, \mathbf{X}_n) \mathbf{K}_{n,n}^{-1} (\mathbf{y} - \tilde{\mathbf{f}}_n)}_{\text{decoupled approximate posterior}}. \quad (34)$$

On the right, the cross-covariance term  $\phi(\cdot)^\top \Phi_n^\top = \phi(\cdot)^\top \phi(\mathbf{X}_n)$  is replaced by  $k(\cdot, \mathbf{X}_n)$ . Seeing as the former is often chosen to approximate the latter in a way that converges when an appropriate limit is taken, for instance in (22), it comes as no surprise that  $k(\cdot, \mathbf{X}_n)$  more accurately represents data. Moreover, the matrix inverse  $(\Phi_n \Phi_n^\top)^{-1}$  appearing on the left is often ill-conditioned and, therefore, amplifies numerical errors. Finite-dimensional GPs constructed from local basis functions exhibit similar issues, albeit for essentially the opposite reason. Rather than failing to adequately represent the data, local basis functions struggle to reproduce the prior.

Many approaches to approximating Gaussian processes  $f \sim \mathcal{GP}(0, k)$  revolve around representing the data in terms of  $m$ -dimensional canonical bases  $k(\cdot, \mathbf{Z})$ ; for a review, see Quiñonero-Candela et al. (2007). Early iterations of this strategy (Silverman, 1985; Wahba, 1990; Tipping, 2000), typically used  $k(\cdot, \mathbf{Z})$  to define degenerate Gaussian processes (Rasmussen and Williams, 2006). Here, the term *degenerate* emphasizes the fact that the covariance function

$$\tilde{k}(\mathbf{x}_i, \mathbf{x}_j) = k(\mathbf{x}_i, \mathbf{Z}) k(\mathbf{Z}, \mathbf{Z})^{-1} k(\mathbf{Z}, \mathbf{x}_j) \quad (35)$$

of such a process has a finite number of non-zero eigenvalues. From the weight-space perspective, degenerate GPs are Bayesian linear models  $\tilde{f}(\cdot) = k(\cdot, \mathbf{Z}) \mathbf{w}$ , which makes it clear that  $\tilde{f}(\cdot)$  goes to zero as  $k(\cdot, \mathbf{Z}) \rightarrow \mathbf{0}$ . This behavior is particularly troublesome if all  $\mathbf{z} \in \mathbf{Z}$  are positioned near training locations  $\mathbf{X}_n$ : since  $k(\mathbf{x}_*, \mathbf{Z})$  typically vanishes as  $\mathbf{x}_*$  retreats from  $\mathbf{Z}$ , both the prior and the posterior collapse to point masses away from the data.

Instead of focusing on the data, one idea is to start by finding a basis  $k(\cdot, \mathbf{Z})$  capable of accurately reproducing the prior. Accomplishing this feat will require us to use a relatively large number of basis functions, since  $\mathbf{Z}$  will need to effectively cover the (compact) domain  $\mathcal{X}$ . As mentioned in Section 4.1, certain kernels produce special kinds of matrices when evaluated on particular sets. Exploiting these special properties—e.g., by taking the Toeplitz matrices formed when evaluating a stationary product kernel  $k$  on a regularly spaced grid  $\mathbf{Z}$  and embedding them inside of circulant ones (Wood and Chan, 1994; Dietrich and Newsam,

1997)—enables us to drastically reduce the cost of expensive matrix operations, such as multiplies, decompositions, and inverses. Especially when  $\mathcal{X}$  is low dimensional, then, we can use the canonical basis to efficiently approximate the prior.

Kernel interpolation methods (Wilson and Nickisch, 2015; Pleiss et al., 2018) take this idea a step further. Given a set of  $m$  inducing locations  $\mathbf{Z}$ , let  $\boldsymbol{\xi} : \mathcal{X} \rightarrow \mathbb{R}^m$  be a *weight function* (Silverman, 1984) mapping locations  $\mathbf{x}_i$  onto (sparse) weight vectors  $\boldsymbol{\xi}_i$  such that  $k(\mathbf{x}_i, \mathbf{Z}) \approx \boldsymbol{\xi}_i^\top k(\mathbf{Z}, \mathbf{Z})$ . By applying this technique to (35), we can define another Gaussian process  $g \sim \mathcal{GP}(0, c)$  with degenerate covariance  $c(\mathbf{x}_i, \mathbf{x}_j) = \boldsymbol{\xi}_i^\top k(\mathbf{Z}, \mathbf{Z}) \boldsymbol{\xi}_j$ . As a Bayesian linear model, we have  $g(\cdot) = \boldsymbol{\xi}(\cdot)^\top \mathbf{g}_m$ . Notice that process values  $\mathbf{g}_m = g(\mathbf{Z})$  now play the role of random weights  $\mathbf{w}$  and fully determine the behavior of the random function  $g$ . Assuming  $\mathbf{Z}$  was chosen so that  $k(\mathbf{Z}, \mathbf{Z})$  admits convenient structure, random vectors  $\mathbf{g}_m \mid \mathbf{y}$  and, hence, random functions  $(g \mid \mathbf{y})(\cdot)$  can be obtained cheaply (Pleiss et al., 2018). When  $\mathbf{Z}$  is sufficiently dense in  $\mathcal{X}$  (so as to be reasonably close to  $\mathbf{x}_*$ ), this strategy provides an alternative means of efficiently sampling from GP posteriors.

## 5.6 An empirical study

By now, we have explored a variety of techniques for sampling from GP posteriors. Each of these methods is well suited for a particular type of problem. To help shed light on their respective niches, we conducted a simple controlled experiment.

Here, our goal is to better understand how different methods balance the tradeoff of cost and accuracy. We measured cost in terms of runtimes and accuracy in terms of 2-Wasserstein distances between empirical distributions and true posterior (see Section 6). To eliminate confounding variables, we assumed a known Matérn-5/2 prior on random functions  $f : \mathbb{R}^4 \rightarrow \mathbb{R}$ . All trials began by sampling this prior at  $n$  training locations  $\mathbf{X}_n$  and 1024 test locations  $\mathbf{X}_*$ , using either location-scale transforms or random Fourier features. We then used the various update rules explored in this section to condition on  $n$  observations  $\mathbf{y} \sim \mathcal{N}(\mathbf{f}_n, 10^{-3}\mathbf{I})$ .

Sparse updates were constructed using  $m = \frac{n}{4}$  inducing variables  $\mathbf{u}$ , whose distributions  $q(\mathbf{u})$  and inducing locations  $\mathbf{Z}$  were obtained by minimizing Kullback–Leibler divergences. Conjugate-gradient-based updates were carried out by, first, computing partial pivoted Cholesky decompositions in order to precondition linear systems  $(\mathbf{K}_{n,n} + \sigma^2 \mathbf{I})\mathbf{v} = (\mathbf{y} - \mathbf{f}_n - \boldsymbol{\varepsilon})$ . We then iteratively solved for Gaussian pathwise updates using the method of conjugate gradients. Stopping conditions for both the partial pivoted Cholesky decomposition and conjugate gradient solver were chosen to match those of Gardner et al. (2018). Prior to discussing trends in Figure 5, we would like to point out that curves associated with Gaussian updates (black) are heavily obscured: in the left column, by CG-based ones (orange and red) and in top middle and top right plots by RFF-based ones (green).

Comparing the rows of Figure 5, we see that random Fourier feature (RFF) approximations to priors introduce modest amounts of error in exchange for large cost reductions. These savings are particularly dramatic in cases where test inputs  $\mathbf{X}_*$  significantly outnumber training locations  $\mathbf{X}_n$ . Echoing discussion in Section 4.5, however,  $m$ -dimensional random Fourier bases struggle to represent the data. All other things being held equal, sparse updates performed in the canonical basis consistently outperform RFF-based ones. These sparse methods are also considerable faster than competing approaches when  $m \ll n$ .

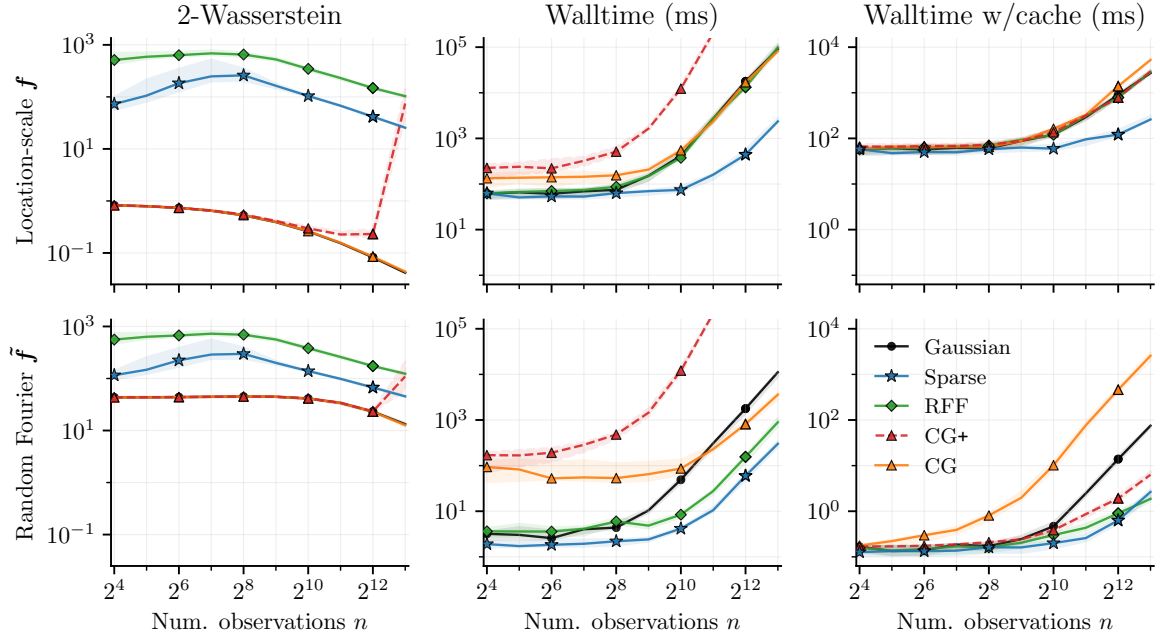


Figure 5: Accuracy and cost of different methods for sampling from GP posteriors given  $n$  observations. Draws from the prior are generated using either location-scale (*top*) or  $\ell = 4096$  random Fourier features (*bottom*). We denote Gaussian updates by black dots, sparse updates by blue stars, CG updates by orange and red triangles, and RFF updates by green diamonds. Sparse and RFF updates both utilized  $m = \frac{n}{4}$  basis functions. All results are reported as medians and interquartile ranges measured over 32 independent trials. *Left*: 2-Wasserstein distances of empirical distributions of  $10^5$  samples from the ground truth GP posterior. *Middle and right*: Time taken to generate a draw of  $(\mathbf{f}_* | \cdot) \in \mathbb{R}^{1024}$  with and without caching of terms that are independent of  $\mathbf{X}_*$ .

Direct comparison of sparse and CG updates is difficult, since both methods are sensitive to various design choices. In our experiments, CG-based updates behaved tantamount to exact ones—with two important caveats. First, CG-based updates were initially slower than exact ones but outpace them as  $n$  increased. Second, naïvely computing pathwise updates using CG is highly inefficient when it comes to caching. When repeatedly conditioning on (potentially different realizations of)  $\boldsymbol{\gamma} = \mathbf{y}$ , one option is to use CG to precompute the matrix inverse  $(\mathbf{K}_{n,n} + \sigma^2 \mathbf{I})^{-1}$ . This CG+ variant is significantly more cache-friendly, but also much more susceptible to round-off error—see dashed red curves in Figure 5.

These empirical results help to characterize the behaviors of errors introduced by different approximation schemes, but leave many questions unanswered. In order to fill in some of the remaining gaps, we now analyze various types of approximation error in details.

## 6. Error analysis

Over the course of this section, we will analyze the different types of error introduced by pathwise approximations. Speaking about these errors requires us to agree upon a

suitable notion of similarity between Gaussian processes. Ultimately, we are interested in understanding how these approximations influence Monte Carlo estimators. We therefore focus on 2-Wasserstein distances between true and approximate posteriors, since they control downstream Monte Carlo errors.<sup>11</sup> These distances measure the similarity of Gaussian processes  $\tilde{f}$  and  $f$  as the expectation of a metric  $d(\tilde{f}, f)$  under the best possible *coupling* of the two processes. Formally, we have

$$W_{2,d}(\tilde{f}, f) = \left[ \inf_{\pi \in \Pi(\tilde{\mu}, \mu)} \mathbb{E}_{\pi} d(\tilde{f}, f)^2 \right]^{1/2}, \quad (36)$$

where  $\Pi(\tilde{\mu}, \mu)$  denotes the set of valid couplings (Mallasto and Feragen, 2017), i.e. joint measures whose marginals correspond with the Gaussian measures  $\tilde{\mu}$  and  $\mu$  induced by processes  $\tilde{f}$  and  $f$ , respectively. Below, we employ  $L^2$  and supremum norms as the underlying metrics used to define 2-Wasserstein distances.

For the remainder of this section, we assume that the domain  $\mathcal{X}$  is a compact subset of some metric measure space  $\mathcal{M}$  and that  $\mathcal{X}$  has finite measure. As a straightforward example, the domain may be a  $d$ -dimensional hypercube  $\mathcal{X} = [a, b]^d$  within  $\mathcal{M} = \mathbb{R}^d$ .

Lastly, let us introduce some additional notation to simplify material presented below. First, we will use  $\tilde{f} \mid \mathbf{y}$  and  $\tilde{f} \mid \mathbf{u}$  to denote pathwise conditioning of an approximate prior  $\tilde{f}$  via canonical (16) and sparse (30) update rules, respectively. These constructions should not be confused with the approximate posteriors discussed in Sections 4.5 and 5.5. Second, we will superscript covariance functions  $k$  to convey their corresponding processes. For example,  $k^{(\tilde{f})}$  will denote the kernel of the approximation prior  $\tilde{f}$ . Third and finally, given a set of  $n$  training locations  $\mathbf{X}_n \subset \mathcal{X}$ , define the *weight function*  $\boldsymbol{\xi} : \mathcal{X} \rightarrow \mathbb{R}^n$  as

$$\boldsymbol{\xi}(\cdot) = k(\mathbf{X}_n, \mathbf{X}_n)^{-1} k(\mathbf{X}_n, \cdot). \quad (37)$$

Variants of this function have been extensively studied in the context of regression; see Silverman (1984) and Sollich and Williams (2005) and references contained therein.

## 6.1 Posterior approximation errors

This section adapts the results of Wilson et al. (2020) to study the error in the decoupled approximate posterior

$$(\tilde{f} \mid \mathbf{y})(\cdot) \triangleq \tilde{f}(\cdot) + k(\cdot, \mathbf{X}_n) \mathbf{K}_{n,n}^{-1} (\mathbf{y} - \tilde{\mathbf{f}}) = \tilde{f}(\cdot) + \boldsymbol{\xi}(\cdot)^{\top} (\mathbf{y} - \tilde{\mathbf{f}}) \quad (38)$$

formed by updating an  $\ell$ -dimensional approximate priors  $\tilde{f}(\cdot) = \boldsymbol{\phi}(\cdot)^{\top} \mathbf{w}$  via an  $n$ -dimensional canonical basis  $k(\cdot, \mathbf{X}_n)$  so as to satisfy the condition imposed by  $n$  noise-free observations  $\mathbf{y}$ .

**Proposition 5** *Assume that  $\mathcal{X} \subset \mathbb{R}^d$  is compact and that the stationary kernel  $k$  is sufficiently regular for  $f \sim \mathcal{GP}(\mu, k)$  to be almost surely continuous. Accordingly, if we define  $C_1 = \sqrt{2} \text{diam}(\mathcal{X})^{d/2} (1 + \|k\|_{\mathcal{C}(\mathcal{X}^2)}^2 \|\mathbf{K}_{n,n}^{-1}\|_{L(\ell^\infty; \ell^1)}^2)^{1/2}$ , then we have*

$$W_{2,L^2(\mathcal{X})}(\tilde{f} \mid \mathbf{y}, f \mid \mathbf{y}) = \left( \inf_{\pi \in \Pi(\tilde{\mu}, \mu)} \mathbb{E}_{\pi} \left\| (\tilde{f} \mid \mathbf{y}) - (f \mid \mathbf{y}) \right\|_{L^2(\mathcal{X})}^2 \right)^{1/2} \leq C_1 W_{2,\mathcal{C}(\mathcal{X})}(\tilde{f}, f), \quad (39)$$

11. 2-Wasserstein distances majorize 1-Wasserstein distances, which regulate expectations of Lipschitz functionals by Kantorovich–Rubinstein duality (Villani, 2008).

where  $W_{2,L^2(\mathcal{X})}$  and  $W_{2,\mathcal{C}(\mathcal{X})}$  respectively denote 2-Wasserstein distances over the Lebesgue space  $L^2(\mathcal{X})$  and the space of continuous functions  $\mathcal{C}(\mathcal{X})$  equipped with the supremum norm,  $\|\cdot\|_{\mathcal{C}(\mathcal{X}^2)}$  is the supremum norm over continuous functions, and  $\|\cdot\|_{L(\ell^\infty;\ell^1)}$  is the operator norm between  $\ell^\infty$  and  $\ell^1$  spaces.

**Proof** We begin by considering the term inside the expectation in (39). Applying Matheron's rule followed by Hölder's inequality ( $p = 1$ ,  $q = \infty$ ), we have

$$\begin{aligned} \left| (\tilde{f} \mid \mathbf{y})(\mathbf{x}) - (f \mid \mathbf{y})(\mathbf{x}) \right|^2 &\leq 2 \left| \tilde{f}(\mathbf{x}) - f(\mathbf{x}) \right|^2 + 2 \left| \boldsymbol{\xi}(\mathbf{x})^\top (\tilde{\mathbf{f}}_n - \mathbf{f}_n) \right|^2 \\ &\leq 2 \left\| \tilde{f} - f \right\|_{L^\infty(\mathcal{X})}^2 + 2 \left\| \boldsymbol{\xi}(\mathbf{x}) \right\|_{\ell^1}^2 \left\| \tilde{\mathbf{f}}_n - \mathbf{f}_n \right\|_{\ell^\infty}^2. \end{aligned} \quad (40)$$

Continuing from the second line, the definition of the operator norm implies that

$$\begin{aligned} \left| (\tilde{f} \mid \mathbf{y})(\mathbf{x}) - (f \mid \mathbf{y})(\mathbf{x}) \right|^2 &\leq 2 \left( 1 + \left\| k(\mathbf{x}, \mathbf{X}_n) \right\|_{\ell^\infty}^2 \left\| \mathbf{K}_{n,n}^{-1} \right\|_{L(\ell^\infty;\ell^1)}^2 \right) \left\| \tilde{f} - f \right\|_{L^\infty(\mathcal{X})}^2 \\ &\leq 2 \left( 1 + \left\| k \right\|_{\mathcal{C}(\mathcal{X}^2)}^2 \left\| \mathbf{K}_{n,n}^{-1} \right\|_{L(\ell^\infty;\ell^1)}^2 \right) \left\| \tilde{f} - f \right\|_{L^\infty(\mathcal{X})}^2 \\ &= \underbrace{2 \left( 1 + \left\| k \right\|_{\mathcal{C}(\mathcal{X}^2)}^2 \left\| \mathbf{K}_{n,n}^{-1} \right\|_{L(\ell^\infty;\ell^1)}^2 \right)}_{C_0} \left\| \tilde{f} - f \right\|_{\mathcal{C}(\mathcal{X})}^2, \end{aligned} \quad (41)$$

where, in the final line, we have used continuity of sample paths to replace  $\|\cdot\|_{L^\infty(\mathcal{X})}$  with  $\|\cdot\|_{\mathcal{C}(\mathcal{X})}$ . We now lift this bound between sample paths to one on 2-Wasserstein distances by integrating both sides with respect to the optimal coupling  $\pi \in \Pi(\tilde{\mu}, \mu)$

$$\begin{aligned} W_{2,L^2(\mathcal{X})}(\tilde{f} \mid \mathbf{y}, f \mid \mathbf{y}) &= \left( \inf_{\pi \in \Pi(\tilde{\mu}, \mu)} \mathbb{E}_\pi \left\| (\tilde{f} \mid \mathbf{y}) - (f \mid \mathbf{y}) \right\|_{L^2(\mathcal{X})}^2 \right)^{1/2} \\ &\leq \left( C_0 \text{vol}(\mathcal{X}) \inf_{\pi \in \Pi(\tilde{\mu}, \mu)} \mathbb{E}_\pi \left\| \tilde{f} - f \right\|_{\mathcal{C}(\mathcal{X})}^2 \right)^{1/2} \\ &\leq C_1 W_{2,\mathcal{C}(\mathcal{X})}(\tilde{f}, f), \end{aligned} \quad (42)$$

where  $\text{vol}(\mathcal{X})$  denotes the Lebesgue measure of  $\mathcal{X}$ . Hence, the claim follows.<sup>12</sup> ■

**Proposition 6** *With the same assumptions, let  $C_2 = n(1 + \|\mathbf{K}_{n,n}^{-1}\|_{\mathcal{C}(\mathcal{X}^2)} \|k\|_{\mathcal{C}(\mathcal{X}^2)})^2$ . Then,*

$$\mathbb{E}_\Phi \left\| k(\tilde{f} \mid \mathbf{y}) - k(f \mid \mathbf{y}) \right\|_{\mathcal{C}(\mathcal{X}^2)} \leq C_2 \mathbb{E}_\Phi \left\| k(\tilde{f}) - k \right\|_{\mathcal{C}(\mathcal{X}^2)}. \quad (43)$$

Moreover, when  $\tilde{f}$  is a random Fourier feature approximation of the prior, it follows that

$$\mathbb{E}_\Phi \left\| k(\tilde{f} \mid \mathbf{y}) - k(f \mid \mathbf{y}) \right\|_{\mathcal{C}(\mathcal{X}^2)} \leq \ell^{-1/2} C_2 C_3, \quad (44)$$

where  $C_3$  is one of several possible constants given by Sutherland and Schneider (2015).

<sup>12</sup>. Note that, since  $f$  is sample-continuous and  $\mathcal{C}(\mathcal{X})$  is a separable metric space,  $W_{2,\mathcal{C}(\mathcal{X})}$  is a proper metric.



**Proof** Let  $M_k : \mathcal{C}(\mathcal{X} \times \mathcal{X}) \rightarrow \mathcal{C}(\mathcal{X} \times \mathcal{X})$  be the bounded linear operator given by

$$(M_k c)(\mathbf{x}, \mathbf{x}') = c(\mathbf{x}, \mathbf{x}') - c(\mathbf{x}, \mathbf{X}_n) \boldsymbol{\xi}(\mathbf{x}') - \boldsymbol{\xi}(\mathbf{x})^\top c(\mathbf{X}_n, \mathbf{x}') + \boldsymbol{\xi}(\mathbf{x})^\top c(\mathbf{X}_n, \mathbf{X}_n) \boldsymbol{\xi}(\mathbf{x}'). \quad (45)$$

Henceforth, we omit the subscript from  $M_k$  to ease notation. Note that, by construction,

$$k^{(f|\mathbf{y})}(\mathbf{x}, \mathbf{x}') = (Mk)(\mathbf{x}, \mathbf{x}') \quad k^{(\tilde{f}|\mathbf{y})}(\mathbf{x}, \mathbf{x}') = (Mk^{(\tilde{f})})(\mathbf{x}, \mathbf{x}'). \quad (46)$$

Focusing on the integrand on the left-hand side of (43), we begin by separating out the operator norm  $\|M\|_{L(\mathcal{C}(\mathcal{X}^2); \mathcal{C}(\mathcal{X}^2))}$  as

$$\left\| k^{(\tilde{f}|\mathbf{y})} - k^{(f|\mathbf{y})} \right\|_{\mathcal{C}(\mathcal{X}^2)} = \left\| Mk^{(\tilde{f})} - Mk \right\|_{\mathcal{C}(\mathcal{X}^2)} \leq \|M\|_{L(\mathcal{C}(\mathcal{X}^2); \mathcal{C}(\mathcal{X}^2))} \left\| k^{(\tilde{f})} - k \right\|_{\mathcal{C}(\mathcal{X}^2)}. \quad (47)$$

Refining this inequality requires us to upper bound  $\|M\|_{L(\mathcal{C}(\mathcal{X}^2); \mathcal{C}(\mathcal{X}^2))}$ . To do so, we write

$$\|Mc\|_{\mathcal{C}(\mathcal{X}^2)} \leq \|c\|_{\mathcal{C}(\mathcal{X}^2)} + 2\|c(\cdot, \mathbf{X}_n) \boldsymbol{\xi}(\cdot)\|_{\mathcal{C}(\mathcal{X}^2)} + \left\| \boldsymbol{\xi}(\cdot)^\top c(\mathbf{X}_n, \mathbf{X}_n) \boldsymbol{\xi}(\cdot) \right\|_{\mathcal{C}(\mathcal{X}^2)}. \quad (48)$$

We now use Hölder's inequality ( $p = 1, q = \infty$ ) followed by the definition of the operator norm  $\|\cdot\|_{L(\ell^\infty; \ell^1)}$  to bound the second and third terms on the right as

$$\begin{aligned} \|c(\cdot, \mathbf{X}_n) \boldsymbol{\xi}(\cdot)\|_{\mathcal{C}(\mathcal{X}^2)} &= \sup_{\mathbf{x}, \mathbf{x}' \in \mathcal{X}} [c(\mathbf{x}, \mathbf{X}_n) \boldsymbol{\xi}(\mathbf{x}')] \\ &\leq \sup_{\mathbf{x}, \mathbf{x}' \in \mathcal{X}} \left[ \|c(\mathbf{x}, \mathbf{X}_n)\|_{\ell^\infty} \|\mathbf{K}_{n,n}^{-1}\|_{L(\ell^\infty; \ell^1)} \|k(\mathbf{X}_n, \mathbf{x}')\|_{\ell^\infty} \right] \\ &\leq \|c\|_{\mathcal{C}(\mathcal{X}^2)} \|\mathbf{K}_{n,n}^{-1}\|_{L(\ell^\infty; \ell^1)} \|k\|_{\mathcal{C}(\mathcal{X}^2)} \end{aligned} \quad (49)$$

and

$$\left\| \boldsymbol{\xi}(\cdot)^\top c(\mathbf{X}_n, \mathbf{X}_n) \boldsymbol{\xi}(\cdot) \right\|_{\mathcal{C}(\mathcal{X}^2)} \leq n \|c\|_{\mathcal{C}(\mathcal{X}^2)} \|\mathbf{K}_{n,n}^{-1}\|_{L(\ell^\infty; \ell^1)}^2 \|k\|_{\mathcal{C}(\mathcal{X}^2)}^2. \quad (50)$$

Returning to (48), we may now bound  $\|Mc\|_{\mathcal{C}(\mathcal{X}^2)}$  by writing

$$\begin{aligned} \|Mc\|_{\mathcal{C}(\mathcal{X}^2)} &\leq \|c\|_{\mathcal{C}(\mathcal{X}^2)} \left( 1 + 2\|\mathbf{K}_{n,n}^{-1}\|_{L(\ell^\infty; \ell^1)} \|k\|_{\mathcal{C}(\mathcal{X}^2)} + n\|\mathbf{K}_{n,n}^{-1}\|_{L(\ell^\infty; \ell^1)}^2 \|k\|_{\mathcal{C}(\mathcal{X}^2)}^2 \right) \\ &\leq \|c\|_{\mathcal{C}(\mathcal{X}^2)} \left( n \left[ 1 + \|\mathbf{K}_{n,n}^{-1}\|_{L(\ell^\infty; \ell^1)} \|k\|_{\mathcal{C}(\mathcal{X}^2)} \right]^2 \right), \end{aligned} \quad (51)$$

which immediately implies that

$$\|M\|_{L(\mathcal{C}(\mathcal{X}^2); \mathcal{C}(\mathcal{X}^2))} = \sup_{c \neq 0} \frac{\|Mc\|_{\mathcal{C}(\mathcal{X}^2)}}{\|c\|_{\mathcal{C}(\mathcal{X}^2)}} \leq n \left[ 1 + \|\mathbf{K}_{n,n}^{-1}\|_{L(\ell^\infty; \ell^1)} \|k\|_{\mathcal{C}(\mathcal{X}^2)} \right]^2. \quad (52)$$

Note that, since this bound is independent of the particular realization of the  $\ell$ -dimensional random Fourier basis  $\phi$  used to construct the approximate prior  $\tilde{f}$ , it is constant with respect to the expectation (43). Finally, Sutherland and Schneider (2015) have shown that there exists a constant  $C_3$  such that

$$\mathbb{E}_\phi \|k^{(\tilde{f})} - k\|_{\mathcal{C}(\mathcal{X}^2)} \leq \ell^{-1/2} C_3. \quad (53)$$

Combining this inequality with the preceding ones gives the result.  $\blacksquare$

Together, Propositions 5 and 6 show that error in the approximate prior  $\tilde{f}$  controls the error in the resulting approximate posterior  $\tilde{f} \mid \mathbf{y}$ . These bounds are not tight, seeing as constants  $C_1$  and  $C_2$  both depend on and may grow with the number of observations  $n$ . Based on this observation, it is tempting to think that the error in  $\tilde{f} \mid \mathbf{y}$  therefore increases in  $n$ . Empirically, however, the opposite trend is observed: the error in  $\tilde{f} \mid \mathbf{y}$  actually diminishes as  $n$  grows (Wilson et al., 2020). To better understand this behavior, we now study the conditions under which a pathwise update may counteract the error introduced by an approximate prior.

## 6.2 Contraction of approximate posteriors with noise-free observations

This section formalizes the following syllogism: (i) the true posterior  $f \mid \mathbf{y}$  and the approximate posterior  $\tilde{f} \mid \mathbf{y}$  have the same mean; (ii) as  $n$  increases, both posteriors contract to their respective means; (iii) therefore, as  $n$  increases, the error introduced by the approximate prior  $\tilde{f}$  washes out.

To begin, let  $\phi : \mathcal{M} \rightarrow \mathbb{R}^\ell$  be an  $\ell$ -dimensional feature map on an ambient space  $\mathcal{M}$  consisting of linearly independent basis functions  $\phi_i$ . We will say that  $\tilde{f}$  is a *standard normal Bayesian linear model* if it admits the representation

$$\tilde{f}(\cdot) = \sum_{i=1}^{\ell} w_i \phi_i(\cdot) \quad w_i \sim \mathcal{N}(0, 1). \quad (54)$$

This description includes the Karhunen–Loève and Fourier feature approximations described in Section 4. As before, let  $\Phi_n = \phi(\mathbf{X}_n)$  be an  $n \times \ell$  feature matrix and  $\mathcal{H}_k$  be the reproducing kernel Hilbert space associated with a kernel  $k$ . We say that a function  $\phi_i$  *lies locally* in  $\mathcal{H}_k$  for a compact  $\mathcal{X} \subseteq \mathcal{M}$  if there exists a function  $\psi_j \in \mathcal{H}_k$  that agrees with  $\phi_i$  on  $\mathcal{X}$ , i.e.  $\phi_i|_{\mathcal{X}} = \psi_j|_{\mathcal{X}}$ .

When  $\mathcal{M}$  is a compact metric space, the eigenfunctions  $\phi_i$  used to construct (truncated) Karhunen–Loève expansions belong to  $\mathcal{H}_k$  by construction. More generally, assessing whether or not  $\phi_i$  lies locally in  $\mathcal{H}_k$  is often straightforward for kernels with known reproducing kernel Hilbert spaces. As a concrete example, the RKHS of a Matérn- $\nu$  kernel is the Sobolev space of order  $\kappa = \nu + d/2$ . For integer values of  $\kappa$ , this is the space of square-integrable functions with  $\kappa$  square-integrable weak derivatives. Trigonometric basis functions  $\phi_i(\mathbf{x}) = \cos(2\pi\boldsymbol{\omega}_i^\top \mathbf{x} + \tau_i)$  can readily be adapted to satisfy this requirement. Specifically, we may multiply them by a suitably chosen, infinitely-differentiable function that ensures they decay to zero outside of  $\mathcal{X}$ , such that the resulting basis functions (and their derivatives) are square-integrable.

We are now ready to state and prove the primary claim. In the following, Proposition 7 and Corollary 8 will demonstrate that  $\tilde{f} \mid \mathbf{y}$  contracts at the same rate as  $f \mid \mathbf{y}$ . Subsequently, Corollary 9 will show that the error in  $\tilde{f} \mid \mathbf{y}$  vanishes as  $n \rightarrow \infty$  in any reasonable limit where the variance of the true posterior contracts to zero everywhere on  $\mathcal{X}$ .

**Proposition 7** *Suppose  $\mathcal{X} \subseteq \mathcal{M}$  is compact and that each of the  $\ell$  basis functions  $\phi_i$  used to construct the standard normal Bayesian linear model  $\tilde{f}$  lies locally in  $\mathcal{H}_k$ . If the points*

$\mathbf{X}_n \subset \mathcal{X}$  used to condition the approximate posterior  $\tilde{f} \mid \mathbf{y}$  are chosen such that  $f \mid \mathbf{y}$  satisfies  $\sup_{\mathbf{x} \in \mathcal{X}} k^{(f|\mathbf{y})}(\mathbf{x}, \mathbf{x}) \leq \varepsilon$ , then it follows that<sup>13</sup>

$$\sup_{\mathbf{x} \in \mathcal{X}} |k^{(\tilde{f}|\mathbf{y})}(\mathbf{x}, \mathbf{x})| \leq C_4 \varepsilon, \quad (55)$$

where we have defined  $C_4 = \ell \max_i \inf \left\{ \|\psi_i\|_{\mathcal{H}_k}^2 : \psi_i|_{\mathcal{X}} = \phi_i|_{\mathcal{X}}, \forall \psi_i \in \mathcal{H}_k \right\}$ .

**Proof** Recall from (38) we can use the weight function  $\boldsymbol{\xi}(\cdot) = k(\mathbf{X}_n, \mathbf{X}_n)^{-1} k(\mathbf{X}_n, \cdot)$  to express the approximate posterior as  $(\tilde{f} \mid \mathbf{y})(\cdot) \stackrel{d}{=} \phi(\cdot)^\top \mathbf{w} - \boldsymbol{\xi}(\cdot)^\top (\mathbf{y} - \boldsymbol{\Phi}_n \mathbf{w})$ . Under this notation, it is clear that we may immediately upper bound the variance of the  $\tilde{f} \mid \mathbf{y}$  as

$$\text{Var}\left((\tilde{f} \mid \mathbf{y})(\cdot)\right) = \mathbb{E}\left[\left(\phi(\cdot)^\top - \boldsymbol{\xi}(\cdot)^\top \boldsymbol{\Phi}_n\right) \mathbf{w}\right]^2 \leq \ell \max_i \left(\phi_i(\cdot) - \boldsymbol{\xi}(\cdot)^\top \phi_i(\mathbf{X}_n)\right)^2, \quad (56)$$

where, on the right, we have used the fact that  $\mathbb{E}\|\mathbf{w}\|^2 = \ell$ . By further denoting  $\mathcal{G} = \{g \in \mathcal{H}_k : \|g\|_{\mathcal{H}_k} = 1\}$ , we may now exploit the dual representation of the RKHS norm to write

$$\begin{aligned} \left| \phi_i(\mathbf{x}_*) - \boldsymbol{\xi}(\mathbf{x}_*)^\top \phi_i(\mathbf{X}_n) \right| &\leq \|\phi_i\|_{\mathcal{H}_k} \sup_{g \in \mathcal{G}} \left| g(\mathbf{x}_*) - \boldsymbol{\xi}(\mathbf{x}_*)^\top g(\mathbf{X}_n) \right| \\ &= \|\phi_i\|_{\mathcal{H}_k} \left\| k(\cdot, \mathbf{x}_*) - \boldsymbol{\xi}(\mathbf{x}_*)^\top \mathbf{K}_{n,*} \right\|_{\mathcal{H}_k} \\ &= \|\phi_i\|_{\mathcal{H}_k} \sqrt{\underbrace{k(\mathbf{x}_*, \mathbf{x}_*) - \mathbf{K}_{*,n} \mathbf{K}_{n,n}^{-1} \mathbf{K}_{n,*}}_{\mathcal{P}_{\mathbf{X}}(\mathbf{x}_*)}} \end{aligned} \quad (57)$$

where, because  $\phi_i$  lies locally in  $\mathcal{H}_k$ , we may replace it with any  $\psi_i \in \mathcal{H}_k : \psi_i|_{\mathcal{X}} = \phi_i|_{\mathcal{X}}$ . Noting that  $\mathcal{P}_{\mathbf{X}}(\cdot) = \sqrt{k^{(f|\mathbf{y})}(\cdot, \cdot)}$  and collecting terms gives the result.  $\blacksquare$

**Corollary 8** *With the same assumptions, as  $\sup_{\mathbf{x} \in \mathcal{X}} k^{(f|\mathbf{y})}(\mathbf{x}, \mathbf{x}) \rightarrow 0$ , it follows that*

$$\sup_{\mathbf{x}, \mathbf{x}' \in \mathcal{X}} |k^{(\tilde{f}|\mathbf{y})}(\mathbf{x}, \mathbf{x}') - k^{(f|\mathbf{y})}(\mathbf{x}, \mathbf{x}')| \rightarrow 0. \quad (58)$$

**Proof** Begin by applying the triangle inequality to the above and, subsequently, use the Cauchy-Schwartz inequality to bound  $k(\mathbf{x}, \mathbf{x}') \leq \sqrt{k(\mathbf{x}, \mathbf{x})} \sqrt{k(\mathbf{x}', \mathbf{x}')}$ , which gives

$$\begin{aligned} \sup_{\mathbf{x}, \mathbf{x}' \in \mathcal{X}} |k^{(\tilde{f}|\mathbf{y})}(\mathbf{x}, \mathbf{x}') - k^{(f|\mathbf{y})}(\mathbf{x}, \mathbf{x}')| &\leq \sup_{\mathbf{x}, \mathbf{x}' \in \mathcal{X}} |k^{(\tilde{f}|\mathbf{y})}(\mathbf{x}, \mathbf{x}')| + \sup_{\mathbf{x}, \mathbf{x}' \in \mathcal{X}} |k^{(f|\mathbf{y})}(\mathbf{x}, \mathbf{x}')| \\ &\leq \sup_{\mathbf{x} \in \mathcal{X}} |k^{(\tilde{f}|\mathbf{y})}(\mathbf{x}, \mathbf{x})| + \sup_{\mathbf{x} \in \mathcal{X}} |k^{(f|\mathbf{y})}(\mathbf{x}, \mathbf{x})|. \end{aligned} \quad (59)$$

In the final expression, convergence of the former term is given by Proposition 7, while the latter goes to zero by assumption.  $\blacksquare$

13. This result holds even when the weights are not assumed i.i.d., albeit with a slightly different constant.

**Corollary 9** *With the same assumptions, as  $\sup_{\mathbf{x} \in \mathcal{X}} k^{(f|\mathbf{y})}(\mathbf{x}, \mathbf{x}) \rightarrow 0$ , it follows that*

$$W_{2,L^2(\mathcal{X})}(f | \mathbf{y}, \tilde{f} | \mathbf{y}) \rightarrow 0. \quad (60)$$

**Proof** Since  $L^2(\mathcal{X})$  is a normed space and  $\mathbb{E}(f | \mathbf{y}) = \mathbb{E}(\tilde{f} | \mathbf{y})$ , we have that

$$W_{2,L^2(\mathcal{X})}(f | \mathbf{y}, \tilde{f} | \mathbf{y}) = W_{2,L^2(\mathcal{X})}\left(\underbrace{f(\cdot) - \boldsymbol{\xi}(\cdot)^\top f(\mathbf{X}_n)}_{(f|\mathbf{y})_0}, \underbrace{\phi(\cdot)^\top \mathbf{w} - \boldsymbol{\xi}(\cdot)^\top \Phi_n \mathbf{w}}_{(\tilde{f}|\mathbf{y})_0}\right), \quad (61)$$

where  $(f | \mathbf{y})_0$  and  $(\tilde{f} | \mathbf{y})_0$  denote centered processes. Now, let  $\mathbb{0}$  be an almost surely zero stochastic process over  $\mathcal{X}$ . Then, by the triangle inequality,

$$W_{2,L^2(\mathcal{X})}\left((f | \mathbf{y})_0, (\tilde{f} | \mathbf{y})_0\right) \leq W_{2,L^2(\mathcal{X})}\left((f | \mathbf{y})_0, \mathbb{0}\right) + W_{2,L^2(\mathcal{X})}\left((\tilde{f} | \mathbf{y})_0, \mathbb{0}\right). \quad (62)$$

Expanding the definition of Wasserstein distances  $W_{2,L^2(\mathcal{X})}$  before using Tonelli's theorem to change the order of integration gives

$$\begin{aligned} W_{2,L^2(\mathcal{X})}\left((f | \mathbf{y})_0, (\tilde{f} | \mathbf{y})_0\right) &\leq \left(\mathbb{E}\|(f | \mathbf{y})_0 - \mathbb{0}\|_{L^2(\mathcal{X})}^2\right)^{1/2} + \left(\mathbb{E}\|(\tilde{f} | \mathbf{y})_0 - \mathbb{0}\|_{L^2(\mathcal{X})}^2\right)^{1/2} \\ &= \left(\int_{\mathcal{X}} k^{(f|\mathbf{y})}(\mathbf{x}, \mathbf{x}) d\mathbf{x}\right)^{1/2} + \left(\int_{\mathcal{X}} k^{(\tilde{f}|\mathbf{y})}(\mathbf{x}, \mathbf{x}) d\mathbf{x}\right)^{1/2}, \end{aligned} \quad (63)$$

where both terms in the final expression converge to zero by compactness of  $\mathcal{X}$  together with Proposition 7.  $\blacksquare$

Together, these claims demonstrate that the decoupled approximate posterior  $\tilde{f} | \mathbf{y}$ , formed by using the canonical basis  $k(\cdot, \mathbf{X}_n)$  to update a well-specified approximate prior  $\tilde{f}$ , *inherits* the contractive properties of the true posterior  $f | \mathbf{y}$ .

Per the beginning of this section, approximate priors  $\tilde{f}$  defined as standard normal Bayesian linear models with basis functions that lie locally in  $\mathcal{H}_k$  are well-specified. The following counterexample helps clarify what can happen when  $\tilde{f}$  is misspecified. Consider an approximate prior  $\tilde{f} \sim \mathcal{GP}(0, \delta)$  equipped with the Kronecker delta kernel  $\delta$  such that  $\text{Cov}(\tilde{f}(\mathbf{x}_i), \tilde{f}(\mathbf{x}_j)) = 1$  if  $\mathbf{x}_i = \mathbf{x}_j$  and 0 otherwise. Given a finite set of test locations  $\mathbf{X}_* \subset \mathcal{X} \setminus \mathbf{X}_n$ , let  $\boldsymbol{\Xi} = \boldsymbol{\xi}(\mathbf{X}_*)^\top$ . Applying the pathwise update (17) to  $\tilde{f}$ , the posterior covariance is then

$$\text{Cov}(\tilde{f}_* | \mathbf{y}) = \text{Cov}(\tilde{f}_*) + \boldsymbol{\Xi} \text{Cov}(\tilde{f}_n) \boldsymbol{\Xi}^\top - 2 \text{Cov}(\tilde{f}_*, \tilde{f}_n) \boldsymbol{\Xi}^\top = \mathbf{I} + \mathbf{K}_{*,n} \mathbf{K}_{n,n}^{-2} \mathbf{K}_{n,*}. \quad (64)$$

Since the second of the two terms on the right is guaranteed non-negative, the variance of the resulting posterior is bounded from below by 1. For this choice of  $\tilde{f}$ , then, the approximation error inherent to  $\tilde{f} | \mathbf{y}$  does not diminish as  $n$  increases.<sup>14</sup>

14. Contraction of the true posterior is well-studied and has strong ties to the literature on kernel methods. Kanagawa et al. (2018) reviews these connections in greater detail: there, Theorem 5.4 shows how the *power function*  $\mathcal{P}_{\mathbf{X}}$  can be bounded in terms of the fill distance  $h(\mathbf{X}_n) = \sup_{\mathbf{x}_* \in \mathcal{X}} \inf_{\mathbf{x} \in \mathbf{X}_n} \|\mathbf{x}_* - \mathbf{x}\|$ .

### 6.3 Sparse approximation errors

We now examine the error introduced by using a sparse pathwise update (30) to construct an approximate posterior. As notation, we write  $f \mid \mathbf{u}$  and  $\tilde{f} \mid \mathbf{u}$  for the approximate posteriors formed by applying the sparse update to the true prior  $f$  and to the approximate prior  $\tilde{f}$ , respectively. Results discussed here mirror those presented by Wilson et al. (2020). Appealing to the triangle inequality, we have

$$\begin{aligned} W_{2,L^2(\mathcal{X})}(\tilde{f} \mid \mathbf{u}, f \mid \mathbf{y}) &\leq \underbrace{W_{2,L^2(\mathcal{X})}(\tilde{f} \mid \mathbf{u}, f \mid \mathbf{u})}_{\text{error in approximate prior}} + \underbrace{W_{2,L^2(\mathcal{X})}(f \mid \mathbf{u}, f \mid \mathbf{y})}_{\text{error in sparse update}} \\ \mathbb{E}_{\phi} \|k(\tilde{f} \mid \mathbf{u}) - k(f \mid \mathbf{y})\|_{\mathcal{C}(\mathcal{X}^2)} &\leq \mathbb{E}_{\phi} \|k(\tilde{f} \mid \mathbf{u}) - k(f \mid \mathbf{u})\|_{\mathcal{C}(\mathcal{X}^2)} + \|k(f \mid \mathbf{u}) - k(f \mid \mathbf{y})\|_{\mathcal{C}(\mathcal{X}^2)}. \end{aligned} \quad (65)$$

From here, any of the previously presented propositions enable us to control the total error. For the first terms on the right, the same arguments as before lead to the same results; however, the constants involved will change, since the sparse update now assumes the role of the canonical one. The latter terms do not involve the approximate prior and are therefore beyond the scope of our present analysis. Note that similar statements hold for the Gaussian pathwise update (28).

As a final remark, note that we may reduce the total error (65) by incorporating additional basis functions  $k(\cdot, \mathbf{X})$  into the sparse update. Conceptually, the act of *augmenting* a sparse update amounts to replacing  $\mathbf{u} \sim q(\mathbf{u})$  with  $\mathbf{u}' \sim q(\mathbf{u}') = p(\mathbf{f} \mid \mathbf{u})q(\mathbf{u})$ , where  $\mathbf{f}$  are process values at centers  $\mathbf{X}$  (Rasmussen and Quiñonero-Candela, 2005; Quiñonero-Candela et al., 2007). By construction,  $q(\mathbf{u})$  and  $q(\mathbf{u}')$  induce the same posterior on  $f$ . However, because the augmented update utilizes additional basis functions, the error in the induced distribution of  $\tilde{\mathbf{f}}_*$  diminishes. This result follows from the same line of reasoning as before: since  $\mathbb{E}(\mathbf{f}_* \mid \mathbf{u}') = \mathbb{E}(\tilde{\mathbf{f}}_* \mid \mathbf{u}')$ ,  $f \mid \mathbf{u}'$  and  $\tilde{f} \mid \mathbf{u}'$  contract to the same function as  $|\mathbf{u}'| \rightarrow \infty$ . Hence, the approximate prior washes out and the total error decreases.

## 7. Applications

This section examines the practical consequences of pathwise conditioning in terms of a curated set of representative tasks. Throughout, we focus on how pathwise methods for efficiently generating function draws from GP posteriors enable us to overcome common obstacles and open doors for new research. We provide a general framework for pathwise conditioning of Gaussian processes based on GPflow (Matthews et al., 2017).<sup>15</sup>

### 7.1 Optimizing black-box functions

Global optimization revolves around the challenge of efficiently identifying a global minimizer

$$\mathbf{x}_{\min} \in \mathbf{X}_{\min} \qquad \mathbf{X}_{\min} = \arg \min_{\mathbf{x} \in \mathcal{X}} f(\mathbf{x}) \quad (66)$$

of a black-box function  $f : \mathcal{X} \rightarrow \mathbb{R}$ . Since  $f$  is a black box, our understanding of its behavior is limited to a set of observations  $\mathbf{y}$  at locations  $\mathbf{X}_n$ . Gaussian processes are a natural and

15. Code is available online at <https://github.com/j-wilson/GPflowSampling>.

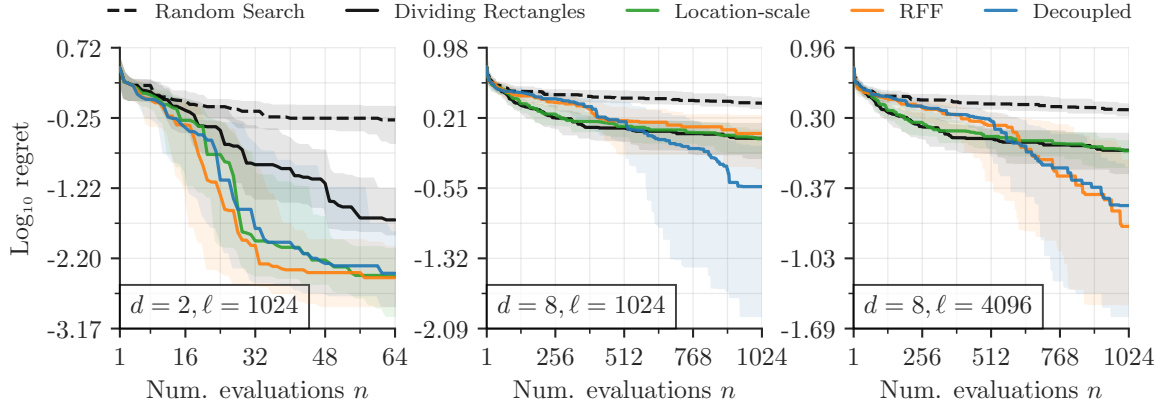


Figure 6: Median performances and interquartile ranges of Thompson sampling methods and popular baselines when optimizing function draws from known GP priors on  $d = \dim(\mathcal{X})$  dimensional domains. Location-scale Thompson sampling performs well in low-dimensional settings (left), but struggles as  $d$  increase due to its inability to efficiently utilize gradient information. RFF posteriors enable us to generate function draws, but demand many more basis functions  $b = \ell + n$  than data points  $n$  (middle vs. right). Decoupled approaches using canonical basis functions  $k(\cdot, \mathbf{x})$  to update RFF priors  $\tilde{f}$  avoids these pitfalls and consistently match or outperform competing strategies.

widely used way of representing possible functions  $f \mid \mathbf{y}$  (Moćkus, 1975; Srinivas et al., 2010; Frazier, 2018). In these cases, we reason about global minimizers (66) in terms of a belief over the random set

$$\mathbf{X}_{\min}^{(f \mid \mathbf{y})} = \arg \min_{\mathbf{x} \in \mathcal{X}} (f \mid \mathbf{y})(\mathbf{x}). \quad (67)$$

Approaches to these problems are often characterized as striking a balance between two competing agendas: the need to learn about the function’s global behavior by *exploring* the domain  $\mathcal{X}$  and the need to obtain (potentially local) minimizers by *exploiting* what is already known.

Thompson sampling is a classic decision-making strategy that balances the tradeoff between exploration and exploitation by sampling actions  $\mathbf{x} \in \mathcal{X}$  in proportion to the probability that  $\mathbf{x} \in \mathbf{X}_{\min}^{(f \mid \mathbf{y})}$  (Thompson, 1933). At first glance, this task may seem daunting, since  $\mathbf{X}_{\min}^{(f \mid \mathbf{y})}$  is random. For a given draw of  $f \mid \mathbf{y}$ , however,  $\mathbf{X}_{\min}^{(f \mid \mathbf{y})}$  is deterministic. Accordingly, we may Thompson sample an action by generating a function  $f \mid \mathbf{y}$  and, subsequently, finding a pathwise global minimizer.

Thompson sampling’s relative simplicity makes it a natural test bed for evaluating different sampling strategies, while its real-world performance (Chapelle and Li, 2011) assures its ongoing relevance in applied settings. A key strength of these methods is that they support embarrassingly-parallel batch selection (Hernández-Lobato et al., 2017; Kandasamy et al., 2018). While many GP-based search strategies allow us to choose  $\kappa > 1$  queries at a time (Snoek et al., 2012; Wilson et al., 2018), their compute costs tend to scale aggressively in  $\kappa$ . Especially when evaluations can be carried out in parallel, then, Thompson sampling provides an affordable alternative to comparable approaches.

We considered three different variants of Thompson sampling, corresponding with different approaches to sampling from GP posteriors. The first approach samples random vectors  $\mathbf{f}_* \mid \mathbf{y}$  using location-scale transforms (19); the second approximates posteriors with Bayesian linear models; and, the third updates function draws from  $\ell$ -dimensional approximate priors  $\tilde{\mathbf{f}} = \boldsymbol{\phi}(\cdot)^\top \mathbf{w}$  using canonical basis functions centered at the  $n$  training locations.<sup>16</sup> For fair comparison, we allocate  $b = \ell + n$  random Fourier basis functions to Bayesian linear models employed by the second approach.

At each round of Thompson sampling, we began by sampling process values  $f_i \mid \mathbf{y}$  independently on a randomly generated discretization of  $\mathcal{X} = [0, 1]^d$ . Next, we constructed a candidate set  $\mathbf{X}_*$  using the locations that produces the smallest realizations of  $f_i \mid \mathbf{y}$ . Under a location-scale approach, we then jointly sampled process values at  $|\mathbf{X}_*| = 2048$  candidates. For both of the alternatives, we instead used  $|\mathbf{X}_*| = 32$  candidates to initialize multi-start gradient descent. In all three cases, queries were chosen as minimizers of the resulting vector  $\mathbf{f}_* \mid \mathbf{y}$ . Batches of queries were obtained using  $\kappa$  independent runs of this algorithm.

To eliminate confounding variables, we experimented with black-box functions drawn from a known Matérn- $5/2$  prior with an isotropic length scale  $l = \sqrt{d/100}$  and Gaussian observations  $y \sim \mathcal{N}(f(\mathbf{x}), 10^{-3})$ . We set  $\kappa = d$ , but this choice was not found to significantly influence our results. Below, we focus on comparing each Thompson sampling variant’s behavior for different amounts of design variables  $d$  and basis functions  $\ell$ .

Figure 6 reports key findings based on 32 independent trials; for extended results, see Wilson et al. (2020). First, location-scale methods’ inability to use gradient information to efficiently find pathwise minimizers causes its performance to wane as  $d$  increases. In contrast, both of the alternative variants of Thompson sampling rely on pathwise-differentiable function draws and, therefore, scale more gracefully in  $d$ . Second, RFF-based Bayesian linear models struggle to represent posteriors due to variance starvation (Section 4.5). As the number of observations  $n$  increases relative to the number of basis functions  $b = \ell + n$ , the function draws they produce come to inadequately characterize the true posterior, causing Thompson sampling to falter. Decoupled approaches to updating  $\tilde{\mathbf{f}}$  avoid this issue by, e.g., associating the data with the  $n$ -dimensional canonical basis  $k(\cdot, \mathbf{X}_n)$ .

## 7.2 Generating boundary-constrained sample paths

This section illustrates how techniques introduced in the preceding sections can be used to efficiently sample Gaussian process posteriors subject to boundary conditions (Solin and Kok, 2019). Whittle (1963) showed that a Matérn GP  $f$  defined over  $\mathbb{R}^d$  satisfies the stochastic partial differential equation

$$\left( \frac{2\nu}{\kappa^2} - \Delta \right)^{\frac{\nu}{2} + \frac{d}{4}} f = \mathcal{W}, \quad (68)$$

where  $\mathcal{W}$  is a (rescaled) white noise process, and  $\Delta$  is the Laplacian. Following Solin and Kok (2019) and Rue and Held (2005), we restrict (68) onto a (well-behaved) compact domain  $\mathcal{X} \subset \mathbb{R}^d$  and impose Dirichlet boundary conditions  $f|_{\partial\mathcal{X}} = 0$  to define a boundary-constrained Matérn Gaussian process over  $\mathcal{X}$ . Solin and Kok (2019) demonstrate that such a prior admits

16. Equation (34) highlights the difference between the second and third approaches.

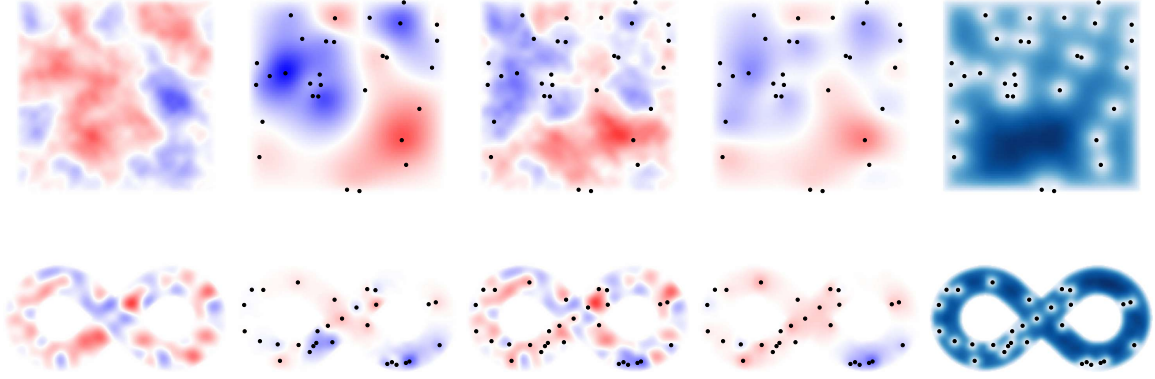


Figure 7: Pathwise conditioning of samples from Matérn priors subject to observations  $\mathbf{y}$  (black dots) and Dirichlet boundary conditions  $f|_{\partial\mathcal{X}} = 0$ . From left to right, the first three columns show a draw from the prior, a pathwise update, and the corresponding realization of the posterior. The final two columns communicate the empirical mean and standard deviation of the posterior, respectively. *Top*: Illustration of a rectangular domain for which Laplacian eigenpairs are calculated analytically. *Bottom*: A non-trivial domain for which the eigenpairs are approximated numerically.

the Karhunen–Loève expansion

$$f(\cdot) = \sum_{i=1}^{\infty} w_i \phi_i(\cdot) \quad w_i \sim \mathcal{N}\left(0, \frac{\sigma^2}{C_\nu} \left(\frac{2\nu}{\kappa^2} + \lambda_i\right)^{-\nu - \frac{d}{2}}\right), \quad (69)$$

where  $\phi_i$  are eigenfunctions of the *boundary-constrained* Laplacian. We truncate this expansion to obtain the  $\ell$ -dimensional Bayesian linear model  $\tilde{f}$ , which we use together with a pathwise update to construct the posterior.

Figure 7 visualizes function draws from boundary-constrained priors and posterior for two choices of boundaries on  $\mathbb{R}^2$ , a rectangle and the symbol for infinity. Note that eigenfunctions for rectangular regions of Euclidean domains are available analytically, while those of the infinity symbol are obtained numerically by solving a Helmholtz equation. Examining this figure, we see that the sample paths respect the Dirichlet boundary condition  $f|_{\partial\mathcal{X}} = 0$ . Karhunen–Loève expansions enable boundary-constrained GPs, an important class of non-stationary priors, to be used within the pathwise conditioning framework.

### 7.3 Simulating dynamical systems

Gaussian process posteriors are commonly used to simulate complex, real-world phenomena in cases where we are unable to actively collect additional data. These phenomena include dynamical systems that describe how physical states evolve over time.

We focus on cases where a Gaussian process prior is placed on the *drift*  $f : \mathcal{X} \times \mathcal{A} \rightarrow \mathcal{X}$  of a time-invariant system, which maps from a state vector  $\mathbf{x}_t \in \mathcal{X}$  and a control input  $\mathbf{a}_t \in \mathcal{A}$  to a tangent vector  $\mathbf{f}_t \in \mathcal{X}$ . Using an Euler–Maruyama scheme to discretize the dynamical



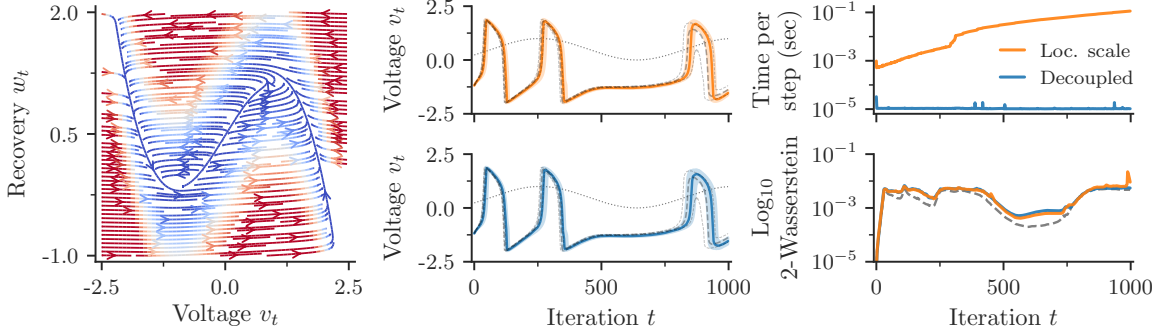


Figure 8: Model-based simulations of a stochastic FitzHugh–Nagumo neuron. *Left*: Phase portrait of the true drift function subject to a fixed current  $a = 0.5$ . *Middle*: Empirical medians and interquartile ranges of simulated voltage traces driven by a sinusoidal current (dotted black); ground truth quartiles are shown in dashed gray. Trajectories generated via location-scale transforms are summarized on the top in orange, while those produced by decoupled drift functions are portrayed on the bottom in blue. *Top right*: Comparison of simulation runtimes. *Bottom right*: Sinkhorn estimates (Cuturi, 2013) to 2-Wasserstein distances between model-based and ground truth state distributions at each step  $t$ . The noise floor (dashed gray) was found using additional ground truth simulations.

system’s equations of motion, we obtain the stochastic difference equation (SDE)

$$\mathbf{x}_{t+1} - \mathbf{x}_t = \tau f(\mathbf{x}_t, \mathbf{a}_t) + \sqrt{\tau} \boldsymbol{\varepsilon}_t = \mathbf{y}_t \quad \boldsymbol{\varepsilon}_t \sim \mathcal{N}(\mathbf{0}, \boldsymbol{\Sigma}_\varepsilon), \quad (70)$$

where  $\tau$  is the chosen step size and  $\boldsymbol{\varepsilon}$  denotes process diffusion. Together with control inputs  $\mathbf{A}_T = (\mathbf{a}_1, \dots, \mathbf{a}_T)$  and diffusion variables  $\mathbf{E}_T = (\boldsymbol{\varepsilon}_1, \dots, \boldsymbol{\varepsilon}_T)$ , each draw of  $f$  fully characterizes how an initial state  $\mathbf{x}_1 \sim p(\mathbf{x}_1)$  evolves over a series of  $T$  successive steps.

Since  $\mathbf{x}_{t+1}$  depends on  $\mathbf{x}_t$ , strategies for jointly sampling  $\mathbf{X}_{T+1} = (\mathbf{x}_1, \dots, \mathbf{x}_{T+1})$  are typically iterative. Under a distributional approach, we generate  $\mathbf{x}_{t+1}$  by sampling from the conditional distribution  $p(\mathbf{y}_t \mid \mathcal{D}_{t-1})$ , where  $\mathcal{D}_{t-1}$  denotes the union of the real data  $(\mathbf{x}_i, \mathbf{y}_i)_{i=1}^n$  and the current trajectory  $(\mathbf{x}_j, \mathbf{y}_j)_{j=1}^{t-1}$ . As mentioned in Section 4.1, we may use low-rank matrix updates to efficiently obtain  $p(\mathbf{y}_t \mid \mathcal{D}_{t-1})$  from  $p(\mathbf{y}_t \mid \mathcal{D}_{t-2})$  in  $\mathcal{O}(t^2)$  time. Nevertheless, the resulting algorithm suffers from  $\mathcal{O}(T^3)$  time complexity. In contrast, approaches based on updating of (approximate) prior function draws scale linearly in  $T$ .

Many of the same issues were explored by Ialongo et al. (2019), who also proposed a linear-time generative strategy for GP-based trajectories. In the language of the present work, this alternative represents the SDE (70) by (i) formulating the unknown drift function as the conditional expectation  $\mathbb{E}(f \mid \mathbf{u}) = k(\cdot, \mathbf{Z}) \mathbf{K}_{m,m}^{-1} \mathbf{u}$  of a sparse Gaussian process  $f$  with inducing variables  $\mathbf{u} \sim q(\mathbf{u})$  and (ii) defining process diffusion as the sum of the remaining terms  $\boldsymbol{\varepsilon}_t \sim \mathcal{N}(\mathbf{0}, k^{(f|\mathbf{u})}(\mathbf{x}_t, \mathbf{x}_t) + \boldsymbol{\Sigma}_\varepsilon)$ . Similar to the pathwise methods put forth here, this approach avoids inter-state dependencies while unrolling by exploiting the fact each draw of  $\mathbf{u}$  realizes an entire drift function.

To better illustrate the practical implications of pathwise approaches to GP-based simulation, we trained a Gaussian process to represent a stochastic variant of the classic FitzHugh–Nagumo model neuron (FitzHugh, 1961; Nagumo et al., 1962). This model

describes a biological neuron in terms of its membrane potential  $v_t$  and a recovery variable  $w_t$  that summarizes the state of its ion channels. Written in the form (70), we have

$$\mathbf{x}_{t+1} - \mathbf{x}_t = \begin{bmatrix} v_{t+1} - v_t \\ w_{t+1} - w_t \end{bmatrix} = \tau \begin{bmatrix} v_t - \frac{v_t^3}{3} - w_t + a_t \\ \frac{1}{\gamma}(v_t - \beta w_t + \alpha) \end{bmatrix} + \sqrt{\tau} \boldsymbol{\varepsilon}_t, \quad (71)$$

where we have chosen  $\tau = 0.25$  ms,  $\alpha = 0.75$ ,  $\beta = 0.75$ ,  $\gamma = 20$ , and  $\boldsymbol{\Sigma}_{\boldsymbol{\varepsilon}} = 10^{-4} \mathbf{I}$ . A two-dimensional phase portrait of this system’s drift function given a current injection  $a = 0.5$  is shown on the left in Figure 8.

Training data was generated by evaluating (71) for  $n = 256$  state-action pairs  $(\mathbf{x}_i, \mathbf{a}_i)$ , chosen uniformly at random from  $\mathcal{X} = [-2.5, 2.5] \times [-1, 2]$  and  $\mathcal{A} = [0, 1]$ . Changes in each of the state variables were modeled by independent, Matérn-5/2 GPs using  $m = 32$  inducing variables. Both sparse GPs were trained by minimizing Kullback–Leibler divergences.

At test time, state trajectories were unrolled from steady state for  $T = 1000$  steps under the influence of a current injection; see middle column of Figure 8. Drift values  $\mathbf{f}_t$  were realized using either the  $\mathcal{O}(T^3)$  location-scale technique or the  $\mathcal{O}(T)$  pathwise approach. As seen on the right in Figure 8, both strategies are capable of accurately characterizing possible state trajectories. At the same time, their difference in cost is striking: the location-scale method spent 10 hours generating 1000 state trajectories (run in parallel), while the pathwise one spent 20 seconds.

## 7.4 Efficiently solving reinforcement learning problems

Model-based approaches to autonomously controlling robotic systems often rely on Gaussian processes to infer system dynamics from a limited number of observations (Rasmussen and Kuss, 2004; Deisenroth et al., 2015; Kamthe and Deisenroth, 2018). Of these data-efficient methods, we focus on PILCO (Deisenroth and Rasmussen, 2011), which is an effective policy search method that uses Gaussian process dynamics models.<sup>17</sup>

Similar to the previous section, we begin by placing a GP prior on the drift function  $f : \mathcal{X} \times \mathcal{A} \rightarrow \mathcal{X}$  of a black-box dynamical system, now assumed to be deterministic. Rather than being given a sequence of actions  $\mathbf{A}_T$  and asked to simulate trajectories  $\mathbf{X}_{T+1}$ , our new goal will be to find parameters  $\boldsymbol{\theta} \in \Theta$  of a deterministic, feedback policy  $\pi : \Theta \times \mathcal{X} \rightarrow \mathcal{A}$  that maximize the expected cumulative reward

$$R(\boldsymbol{\theta}) = \mathbb{E}_{f, \mathbf{x}_1} \left[ \sum_{t=1}^T r \left( \underbrace{\mathbf{x}_t + f(\mathbf{x}_t, \pi_{\boldsymbol{\theta}}(\mathbf{x}_t))}_{\mathbf{x}_{t+1}} \right) \right] = \sum_{t=1}^T \mathbb{E}_{\mathbf{x}_{t+1}} [r(\mathbf{x}_{t+1})]. \quad (72)$$

For suitably chosen reward functions  $r : \mathcal{X} \rightarrow \mathbb{R}$ , we may optimize  $\boldsymbol{\theta}$  by differentiating (72). The challenge, however, is to evaluate this expectation in the first place.

The original PILCO algorithm tackles this problem by using moment matching to approximately propagate uncertainty through time. Given a random state  $\mathbf{x}_t \sim \mathcal{N}(\boldsymbol{\mu}_t, \boldsymbol{\Sigma}_{t,t})$ , we begin by supposing that  $\mathbf{x}_t$  and  $\mathbf{a}_t = \pi_{\boldsymbol{\theta}}(\mathbf{x}_t)$  are jointly normal. Next, we obtain the corresponding optimal Gaussian approximation to  $p(\mathbf{x}_t, \mathbf{a}_t)$  by analytically computing the required moments  $\mathbb{E}(\mathbf{a}_t)$ ,  $\text{Cov}(\mathbf{a}_t, \mathbf{a}_t)$ , and  $\text{Cov}(\mathbf{a}_t, \mathbf{x}_t)$ . This step can also be seen as finding

17. PILCO implementation available separately at <https://github.com/j-wilson/GPflowPILCO>.

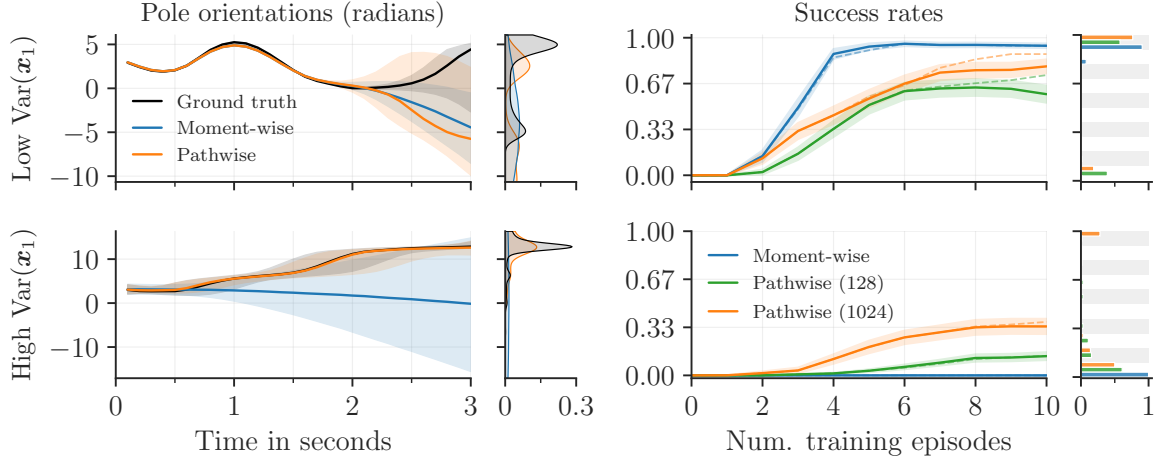


Figure 9: Behavior and performance of PILCO algorithms applied to different versions of cart-pole. Marginal distributions of terminal values are shown immediately to the right of each plot. In top and bottom rows, initial state  $\mathbf{x}_1$  is nearly deterministic and highly randomized, respectively. *Left:* Medians and interquartile ranges of simulated pole orientations. *Right:* Means and standard errors of success rates (estimated separately by unrolling the true system 100 times); dashed lines represent average performances of incumbent policies. On the bottom right, Pathwise ( $s$ ) indicates that  $s$  samples were used during training.

the affine approximation to  $\pi_{\theta}$  that best propagates  $\mathcal{N}(\mu_t, \Sigma_{t,t})$ . We now use moment matching to propagate this approximate joint distribution through  $f$  in order to construct a second Gaussian approximation, this time to  $p(\mathbf{x}_t, \mathbf{f}_t)$ .<sup>18</sup> By interpreting  $\mathbf{x}_{t+1} = \mathbf{x}_t + \mathbf{f}_t$  as the sum of jointly Gaussian random variables, we compute the corresponding right-hand side term of (72) and, finally, proceed to the next time step. Overall, this strategy works well when  $f$  and  $\pi_{\theta}$  are sufficiently regular and  $\mathcal{N}(\mu_t, \Sigma_{t,t})$  is sufficiently peaked that maps from  $\mathbf{x}_t$  to  $\mathbf{f}_t$  are nearly affine in a ball around  $\mu_t$  whose radius is dictated by  $\Sigma_{t,t}$ .

Here, we are interested in comparing the behavior of moment-based and path-based approaches to optimizing (72). To shed light on how these approaches fare in the context of typical learning problems, we experimented with both methods on the *cart-pole* task (Barto et al., 1983), which consists of moving a cart horizontally along a track in order to swing up and balance a pole, upside down, at a target location. State vectors  $\mathbf{x} = [x_0, \dot{x}_0, x_1, \dot{x}_1]^\top$  define the position of the cart  $x_0$ , angle of the pole  $x_1$ , and time derivatives thereof; while, actions  $\mathbf{a} \in \mathcal{A} = [-10, 10]$  N represent the lateral forces applied to the cart.

We follow Deisenroth et al. (2015) by using a 0.5 m long, 0.5 kg pole and a 0.5 kg cart with a 0.1 Ns/m friction coefficient. Each episode ran for a length of 3 seconds, discretized at 0.1 s intervals during which time actions were held constant, i.e., zero-order hold control.

18. By appealing to the affine approximation view of moment matching, we obtain the approximate cross-covariance  $\text{Cov}(\mathbf{x}_t, \mathbf{f}_t) \approx \text{Cov}(\mathbf{x}_t, \mathbf{s}_t) \text{Cov}(\mathbf{s}_t, \mathbf{s}_t)^{-1} \text{Cov}(\mathbf{s}_t, \mathbf{f}_t)$  where  $\mathbf{s}_t = \mathbf{x}_t \oplus \mathbf{a}_t$ .

We set the goal state to  $\mathbf{x}_{\text{goal}} = \mathbf{0}$  and define rewards according to a Gaussian function

$$r(\mathbf{x}) = \exp\left(-\frac{1}{2} \underbrace{(\mathbf{x} - \mathbf{x}_{\text{goal}})^\top \mathbf{\Lambda}^{-1} (\mathbf{x} - \mathbf{x}_{\text{goal}})}_{\substack{\text{sq. Euclidean distance} \\ \text{between pendulum tip and goal}}}\right), \quad (73)$$

whose precision matrix  $\mathbf{\Lambda}^{-1}$  was chosen such that the bracket term is proportional to the squared Euclidean distance between (the Cartesian coordinates of) the tip of the pole in states  $\mathbf{x}$  and  $\mathbf{x}_{\text{goal}}$ . Along the same lines, an episode was considered successful if the tip of the pole was within 0.1 m of the goal for 10 or more consecutive time steps. Depending on the particular experiment, states were initialized in one of two ways: (i) the standard case  $\mathbf{x}_1 \sim \mathcal{N}([0, \pi, 0, 0]^\top, 0.01\mathbf{I})$  or (ii) a challenge variant  $\mathbf{x}_1 \sim \mathcal{N}([0, \pi, 0, 0]^\top, \text{diag}(1, 1, \pi, \pi))$ .

In all cases, system dynamics were represented by a set of independent sparse GPs with squared exponential kernels, each of which predicted a single component of the tangent vector  $\mathbf{f} = f(\mathbf{x}, \mathbf{a})$ . Upon collecting an additional episode of training data, these GPs were trained from scratch using L-BFGS (Liu and Nocedal, 1989) with  $m = \min(n, 256)$  inducing variables, whose corresponding inducing locations  $\mathbf{Z}$  were initialized via  $k$ -means.

We defined policies as kernel regressors with inverse link functions  $g^{-1} : \mathbb{R} \rightarrow [-10, 10]$

$$\pi_{\boldsymbol{\theta}}(\cdot) = g^{-1}\left(\sum_{i=1}^{30} w_i k(\cdot, \mathbf{x}_i)\right) \quad g^{-1}(\cdot) = 20\Phi(\cdot) - 10, \quad (74)$$

where  $k$  denotes a squared exponential kernel and  $\Phi : \mathbb{R} \rightarrow [0, 1]$  is the standard normal CDF. Policy parameters  $\boldsymbol{\theta}$  consisted of centers  $(\mathbf{x}_1, \dots, \mathbf{x}_{30})$ , weights  $\mathbf{w}$ , and length scales  $\mathbf{l}$ . Following Deisenroth et al. (2015), policies were initialized once after collecting a random initial episode and subsequently fine-tuned. At each round,  $\boldsymbol{\theta}$  was updated 5000 times using ADAM (Kingma and Ba, 2015) with gradient norms clipped to one and an initial learning rate 0.01 that decreased by a factor of ten after every third of training. Pathwise approaches propagated uncertainty by unrolling a separate draw of  $\mathbf{x}_1$  along each realization of  $\mathbf{f}$ , both of which were resampled prior to each update of  $\boldsymbol{\theta}$ .

In line with previous findings, moment-wise PILCO consistently solves the standard cart-pole task within a few episodes (Deisenroth et al., 2015). As initial state distributions become increasingly diffuse, however, moment matching struggles to accurately propagate uncertainty. As seen in the bottom row of Figure 9, this inability prevents moment-wise PILCO from learning meaningful policies for the challenge variant of cart-pole. Pathwise alternatives do not experience this issue, but they are not without their own shortcomings. We now discuss relative merits of both approaches to propagating uncertainty.

Pathwise uncertainty propagation is significantly faster than moment matching, enabling us to simulate (tens of) thousands of trajectories in the time it takes to complete a single forward pass of moment matching. As Monte Carlo methods, pathwise estimates of (72) allow us to easily achieve the desired balance of accuracy and cost by controlling the sample size. Here, the use of sampling conveys additional benefits. First, it frees us from the restrictive class of moment matchable models by eliminating the need for closed-form integration. Second, it drastically simplifies implementation and allows us to fully take advantage of modern hardware and software, such as GPUs and automatic differentiation.

On the other hand, we observe that moment-wise uncertainty propagation sometimes improves performance. By locally linearizing the functions it permeates, moment matching implicitly favors simpler, smoother dynamics  $f$  and policies  $\pi_{\theta}$  (see Figure 9). Perhaps for this very reason, moment-wise PILCO was found to train more robustly. In particular, its pathwise counterpart was more susceptible to catastrophic forgetting: after solving the problem during the previous round of training, policies trained via pathwise uncertainty propagation were more likely to diverge. To illustrate this behavior, we define the *incumbent* as the policy that achieves highest expected reward under the model  $f$ . Unlike those of its moment-wise analogue, pathwise PILCO’s incumbents (dashed lines) often outperform more recent policies (solid lines) by significant margins; see right side of Figure 9. While this issue was easy to reproduce, the relatively abundance of moving pieces makes it difficult to pinpoint precisely why it occurs.

Many of the challenges highlighted above are common in reinforcement learning, where generic solutions are often outperformed by skillfully tuned, bespoke alternatives. Nevertheless, we hope that the ease and flexibility of pathwise approaches to simulating posteriors will allow Gaussian processes to be applied to a wide range of problems where data-efficiency and uncertainty calibration are paramount.

## 7.5 Evaluating deep Gaussian processes

When applying Gaussian process methods to novel problems, we are often faced with a natural dilemma: many phenomena of interest are definitively non-Gaussian. In order to leverage Gaussian processes to model these phenomena, we typically resort to nonlinearly transforming  $f$ . Seeing as Gaussian random variables pushed forward through nonlinear functions seldom admit convenient analytic expressions, we are forced to trade tractability for expressivity.

This issue has recently come to the fore in the context of deep Gaussian processes (Damianou and Lawrence, 2013), which represent function priors as compositions

$$f(\cdot) = (f^{(T)} \circ \dots \circ f^{(2)} \circ f^{(1)})(\cdot), \quad (75)$$

where  $f^{(t)} \sim \mathcal{GP}(\mu^{(t)}, k^{(t)})$  for  $t = 1, \dots, T$ . Following Salimbeni and Deisenroth (2017), sample-based methods have become the standard approach for evaluating and training these models. When a composition (75) consists of independent layers made up of independent, scalar-valued GPs (or linear combinations thereof),  $f(\mathbf{x})$  can be efficiently sampled without resorting to expensive matrix operations. When these assumptions are violated, however, sample-based evaluations of deep GPs quickly becomes expensive. One such example was implicitly touched on in preceding sections: Gaussian process models of time-varying stochastic differential equations can be seen as continuous-time analogues of certain deep GPs (Hegde et al., 2019). In these cases, dependencies between successive evaluations of a GP-based drift function  $f^{(t)}(\cdot) = f(t, \cdot)$  cause location-scale based evaluations to grind to halt (see Section 7.3).

Similar issues arise when sampling from compositions of multioutput GPs (van der Wilk et al., 2020). The remainder of this section focuses on the particular case of deep convolutional GPs (Blomqvist et al., 2019; Dutordoir et al., 2020). Here, a deep GP is defined in close analogy to a convolutional neural network (van der Wilk et al., 2017): each layer consists

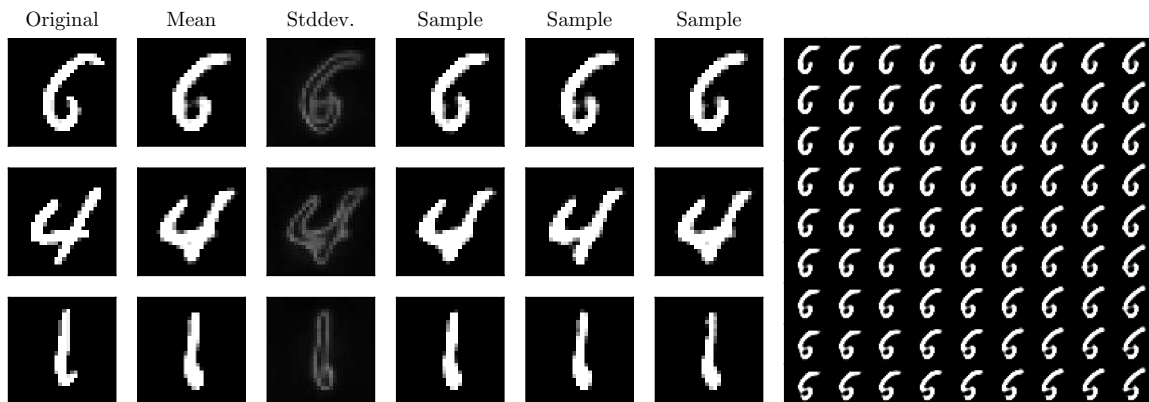


Figure 10: Reconstructions of MNIST digits by a deep convolutional GP trained to act as an autoencoder. *Left*: Mean and standard deviations of the (non-Gaussian) distribution over the reconstructions of randomly chosen test images are shown alongside three independently generated samples. *Right*: A 2-dimensional projection of a 25-dimensional latent space is found by performing SVD on the Jacobian of the mean response of the first decoder layer given an encoding of first image shown on the left. Reconstructions using the mean of each decoder layer are shown for a local walk in this 2-dimensional projected space.

of a set of independent maps that are convolved over local subsets (patches) of an image  $\mathbf{x}_t \in \mathbb{R}^{c_t \times h_t \times w_t}$ . For a convolutional neural network, these *patch response functions* are affine transformations followed by nonlinearities; while, for a convolutional Gaussian process, they are draws from GP posteriors.

Since each of the  $c_t$  independent patch response functions produces  $h_t \times w_t$  output features, the covariance of the Gaussian random variables  $\mathbf{x}_t = \mathbf{f}^{(t-1)} * \mathbf{x}_{t-1}$  is a block diagonal square matrix of order  $c_t \times h_t \times w_t$ . Location-scale approaches to jointly sampling these feature maps incur  $\mathcal{O}(c_t \times h_t^3 \times w_t^3)$  cost when computing matrix square roots.<sup>19</sup> Rather than sampling each layer at the current set of inputs, pathwise strategies sample entire models. Said again, pathwise approaches operate by drawing deterministic models from (approximations to) deep GP posteriors.<sup>20</sup> By doing so, these methods allow us to evaluate individual layers in  $\mathcal{O}(c_t \times h_t \times w_t)$  time.

As an illustrative example, we trained a deep GP to act as an autoencoder for the MNIST dataset (LeCun and Cortes, 2010). For the encoder, we employed a sequence of three convolutional layers, each with 384 inducing patches  $\mathbf{Z} \in \mathbb{R}^{c_{t-1} \times 3 \times 3}$  shared between  $c_t \in (32, 32, 1)$  independent GPs. Strides and padding were chosen to produce a 25-dimensional encoding of a 784-dimensional image. Analogously, we defined the decoder using three transposed convolutional layers, each with 384 inducing patches  $\mathbf{Z} \in \mathbb{R}^{c_{t-1} \times 3 \times 3}$  shared between  $c_t \in (32, 32, 32)$  independent GPs. We then used a final decoder layer, consisting of a single convolutional GP (with the same general outline as above), to resolve penultimate feature maps  $\mathbb{R}^{32 \times 28 \times 28}$  into image reconstructions  $\mathbb{R}^{1 \times 28 \times 28}$ . In all cases, we employ residual connections by using bilinear interpolation to define identity mean functions. Following

19. This cost is separately incurred by each input to each layer, see Dutordoir et al. (2020).

20. Here, we have assumed the use of approximate priors akin to those discussed in Section 4.

Salimbeni and Deisenroth (2017), we initialized inducing patches  $\mathbf{Z}$  using  $k$ -means and inducing distributions to be nearly deterministic.

Model evaluations were performed by using the sparse update (30) together with functions drawn from approximate priors constructed using  $\ell = 256$  random Fourier features. We associate each input image with a single draw of the model. Running on a single GPU, the model outlined above was jointly trained in just over 40 minutes using  $10^4$  steps of gradient descent with a batch size of 128. Figure 10 visualizes the behavior of reconstructions for a randomly chosen set of test images. While this GP-based autoencoder performs fairly well, there is an abundance of open questions regarding deep Gaussian processes in the wild. We hope that the ability to efficiently sample and evaluate draws of composite functions (75) will enable future works to further explore this space.

## 8. Conclusion

Throughout this work, we have used Matheron’s update rule (Theorem 1) as the driving force for looking at Gaussian processes in a different light. This simple equivalence, namely

$$(\mathbf{a} \mid \mathbf{b} = \boldsymbol{\beta}) \stackrel{\text{d}}{=} \mathbf{a} + \boldsymbol{\Sigma}_{\mathbf{a},\mathbf{b}} \boldsymbol{\Sigma}_{\mathbf{b},\mathbf{b}}^{-1} (\boldsymbol{\beta} - \mathbf{b}), \quad (4)$$

allows us to think about GP posteriors at the level of sample paths. Doing so not only helps to clarify existing ideas, but enables us to envision new ones. As it turns out, many of these ideas are intimately practical.

We have repeatedly stressed how pathwise conditioning enables us to separate Gaussian process priors from data-drive updates. We may then leverage these objects’ mathematical properties to construct efficient approximators. As a rule, however, the patterns at play in both cases are fundamentally different: priors typically admit convenient global trends, whereas data often exerts localized influences. Fully exploiting these properties requires us to use different representations, such as different bases, for each of these terms. Decomposing GP posteriors into global and local components makes this particularly easy.

Pathwise and distributional conditioning are complementary viewpoints that lead to complementary methods. In cases where quantities of interest are readily obtained by working with (finite-dimensional) marginals, distributions act as a natural lens for viewing Gaussian process posteriors. On the other hand, when a problem involves arbitrarily many random variables, random functions provide a more direct path to efficient solutions.

All said and done, pathwise conditioning is a powerful tool for both reasoning about and working with GPs. Methods that fit this mold are generally straightforward to use and can easily be tailored to take advantage of a given task’s properties. We have done our best to overview key ingredients for efficiently sampling from Gaussian process posteriors and look forward to learning more about related ideas alongside you, the reader.

## Acknowledgments

We are grateful to Prof. Mikhail Lifshits for his helpful comments regarding the theoretical part of this work. J.T.W. was supported the EPSRC Centre for Doctoral Training in High Performance Embedded and Distributed Systems, reference EP/L016796/1. V.B. and P.M.

were supported by “Native towns”, a social investment program of PJSC Gazprom Neft and by the Ministry of Science and Higher Education of the Russian Federation, agreements № 075-15-2019-1619 and № 075-15-2019-1620. A.T. was supported by the Department of Mathematics at Imperial College London.

## References

- A. G. Barto, R. S. Sutton, and C. W. Anderson. Neuronlike adaptive elements that can solve difficult learning control problems. *IEEE Transactions on Systems, Man, and Cybernetics*, (5):834–846, 1983. Cited on page 35.
- J. Bect, D. Ginsbourger, L. Li, V. Picheny, and E. Vazquez. Sequential design of computer experiments for the estimation of a probability of failure. *Statistics and Computing*, 22(3):773–793, 2012. Cited on page 2.
- K. Blomqvist, S. Kaski, and M. Heinonen. Deep convolutional Gaussian processes. In *Joint European Conference on Machine Learning and Knowledge Discovery in Databases*, pages 582–597. Springer, 2019. Cited on page 37.
- V. Borovitskiy, I. Azangulov, A. Terenin, P. Mostowsky, M. P. Deisenroth, and N. Durrande. Matérn Gaussian processes on graphs. In *Artificial Intelligence and Statistics*, pages 2593–2601, 2021. Cited on page 13.
- V. Borovitskiy, A. Terenin, P. Mostowsky, and M. P. Deisenroth. Matérn Gaussian processes on Riemannian manifolds. In *Advances in Neural Information Processing Systems*, 2020. Cited on page 13.
- D. R. Burt, C. E. Rasmussen, and M. van der Wilk. Convergence of sparse variational inference in Gaussian processes regression. *Journal of Machine Learning Research*, 21(131):1–63, 2020. Cited on page 19.
- D. Calandriello, L. Carratino, A. Lazaric, M. Valko, and L. Rosasco. Gaussian process optimization with adaptive sketching: scalable and no regret. In *Conference on Learning Theory*, pages 533–557, 2019. Cited on page 15.
- P. E. Castro, W. H. Lawton, and E. Sylvestre. Principal modes of variation for processes with continuous sample curves. *Technometrics*, 28(4):329–337, 1986. Cited on page 12.
- J. T. Chang and D. Pollard. Conditioning as disintegration. *Statistica Neerlandica*, 51(3):287–317, 1997. Cited on page 5.
- O. Chapelle and L. Li. An empirical evaluation of Thompson sampling. In *Advances in Neural Information Processing Systems*, pages 2249–2257, 2011. Cited on page 30.
- C.-A. Cheng and B. Boots. Variational inference for Gaussian process models with linear complexity. In *Advances in Neural Information Processing Systems*, pages 5184–5194, 2017. Cited on page 15.



- J.-P. Chilès and P. Delfiner. *Geostatistics: Modeling Spatial Uncertainty*. John Wiley & Sons, 2012. Cited on pages 2, 10.
- J.-P. Chilès and C. Lantuéjoul. Prediction by conditional simulation: models and algorithms. In *Space, Structure and Randomness*, pages 39–68. Springer, 2005. Cited on page 9.
- M. Cuturi. Sinkhorn distances: lightspeed computation of optimal transport. In *Advances in Neural Information Processing Systems*, pages 2292–2300, 2013. Cited on page 33.
- A. Damianou and N. Lawrence. Deep Gaussian processes. In *Artificial Intelligence and Statistics*, pages 207–215, 2013. Cited on page 37.
- C. de Fouquet. Reminders on the conditioning Kriging. In *Geostatistical Simulations*, pages 131–145. Springer, 1994. Cited on page 10.
- M. P. Deisenroth, D. Fox, and C. E. Rasmussen. Gaussian processes for data-efficient learning in robotics and control. *IEEE Transactions on Pattern Analysis and Machine Intelligence*, 37(2):408–423, 2015. Cited on pages 2, 34–36.
- M. P. Deisenroth and C. E. Rasmussen. PILCO: A model-based and data-efficient approach to policy search. In *International Conference on Machine Learning*, pages 465–472, 2011. Cited on page 34.
- C. R. Dietrich and G. N. Newsam. Fast and exact simulation of stationary Gaussian processes through circulant embedding of the covariance matrix. *SIAM Journal of Scientific Computing*, 18:1088–1107, 1997. Cited on pages 11, 20.
- A. Doucet. A note on efficient conditional simulation of Gaussian distributions. Technical report, University of British Columbia, 2010. Cited on page 9.
- N. Durrande, V. Adam, L. Bordeaux, S. Eleftheriadis, and J. Hensman. Banded matrix operators for Gaussian Markov models in the automatic differentiation era. In *Artificial Intelligence and Statistics*, pages 2780–2789, 2019. Cited on page 11.
- V. Dutordoir, M. van der Wilk, A. Artemev, and J. Hensman. Bayesian image classification with deep convolutional Gaussian processes. In *Artificial Intelligence and Statistics*, pages 1529–1539, 2020. Cited on pages 37, 38.
- X. Emery. Conditioning simulations of Gaussian random fields by ordinary Kriging. *Mathematical Geology*, 39(6):607–623, 2007. Cited on page 10.
- L. C. Evans. *Partial Differential Equations*. American Mathematical Society, 2010. Cited on pages 13, 14.
- R. FitzHugh. Impulses and physiological states in theoretical models of nerve membrane. *Biophysical Journal*, 1(6):445, 1961. Cited on page 33.
- P. I. Frazier. A tutorial on Bayesian optimization. *arXiv:1807.02811*, 2018. Cited on page 30.

- K. Fukunaga. *Introduction to Statistical Pattern Recognition*. Elsevier, 2013. Cited on pages 12, 13.
- J. Gardner, G. Pleiss, K. Q. Weinberger, D. Bindel, and A. G. Wilson. GPyTorch: blackbox matrix-matrix Gaussian process inference with GPU acceleration. In *Advances in Neural Information Processing Systems*, pages 7576–7586, 2018. Cited on pages 19, 21.
- A. Grigoryan. *Heat Kernel Analysis on Manifolds*. American Mathematical Society, 2009. Cited on page 13.
- P. Hegde, M. Heinonen, H. Lähdesmäki, and S. Kaski. Deep learning with differential Gaussian process flows. In *Artificial Intelligence and Statistics*, pages 1812–1821, 2019. Cited on page 37.
- J. Hensman, N. Durrande, and A. Solin. Variational Fourier features for Gaussian processes. *Journal of Machine Learning Research*, 18(151):1–151, 2017. Cited on page 15.
- J. Hensman, N. Fusi, and N. D. Lawrence. Gaussian processes for big data. In *Uncertainty in Artificial Intelligence*, pages 282–290, 2013. Cited on page 17.
- J. Hensman, A. Matthews, and Z. Ghahramani. Scalable variational Gaussian process classification. In *Artificial Statistics and Machine Learning*, 2015. Cited on page 17.
- J. M. Hernández-Lobato, J. Requeima, E. O. Pyzer-Knapp, and A. Aspuru-Guzik. Parallel and distributed Thompson sampling for large-scale accelerated exploration of chemical space. In *International Conference on Machine Learning*, pages 1470–1479, 2017. Cited on page 30.
- Y. Hoffman and E. Ribak. Constrained realizations of Gaussian fields: a simple algorithm. *The Astrophysical Journal*, 380:L5–L8, 1991. Cited on page 10.
- A. D. Ialongo, M. van der Wilk, J. Hensman, and C. E. Rasmussen. Overcoming mean-field approximations in recurrent Gaussian process models. In *International Conference on Machine Learning*, pages 2931–2940. PMLR, 2019. Cited on page 33.
- A. G. Journel and C. J. Huijbregts. *Mining Geostatistics*. Academic Press, 1978. Cited on pages 2, 10.
- O. Kallenberg. *Foundations of Modern Probability*. Springer, 2006. Cited on pages 5, 6.
- S. Kamthe and M. P. Deisenroth. Data-efficient reinforcement learning with probabilistic model predictive control. In *Artificial Intelligence and Statistics*, pages 1701–1710, 2018. Cited on page 34.
- M. Kanagawa, P. Hennig, D. Sejdinovic, and B. K. Sriperumbudur. Gaussian processes and kernel methods: A review on connections and equivalences. *arXiv:1807.02582*, 2018. Cited on page 28.

- K. Kandasamy, A. Krishnamurthy, J. Schneider, and B. Póczos. Parallelised Bayesian optimisation via Thompson sampling. In *Artificial Intelligence and Statistics*, pages 133–142, 2018. Cited on page 30.
- D. P. Kingma and J. Ba. Adam: a method for stochastic optimization. In *International Conference on Learning Representations*, 2015. Cited on page 36.
- E. T. Krainski, V. Gómez-Rubio, H. Bakka, A. Lenzi, D. Castro-Camilo, D. Simpson, F. Lindgren, and H. Rue. *Advanced spatial modeling with stochastic partial differential equations using R and INLA*. CRC Press, 2018. Cited on page 13.
- M. Lázaro-Gredilla and A. Figueiras-Vidal. Inter-domain Gaussian processes for sparse inference using inducing features. In *Advances in Neural Information Processing Systems*, pages 1087–1095, 2009. Cited on pages 15, 18.
- Y. LeCun and C. Cortes. MNIST handwritten digit database, 2010. URL: <http://yann.lecun.com/exdb/mnist/>. Cited on page 38.
- M. Lifshits. *Lectures on Gaussian Processes*. Springer, 2012. Cited on page 13.
- F. Lindgren, H. Rue, and J. Lindström. An explicit link between Gaussian fields and Gaussian Markov random fields: the stochastic partial differential equation approach. *Journal of the Royal Statistical Society: Series B (Statistical Methodology)*, 73(4):423–498, 2011. Cited on pages 13, 14.
- D. C. Liu and J. Nocedal. On the limited memory BFGS method for large scale optimization. *Mathematical programming*, 45(1):503–528, 1989. Cited on page 36.
- J. Loper, D. Blei, J. P. Cunningham, and L. Paninski. General linear-time inference for Gaussian Processes on one dimension. *arXiv:2003.05554*, 2020. Cited on page 11.
- G. J. Lord, C. E. Powell, and T. Shardlow. *An Introduction to Computational Stochastic PDEs*. Cambridge University Press, 2014. Cited on pages 13, 14.
- D. G. Luenberger. *Optimization by Vector Space Methods*. John Wiley & Sons, 1997. Cited on page 6.
- A. Mallasto and A. Feragen. Learning from uncertain curves: the 2-Wasserstein metric for Gaussian processes. In *Advances in Neural Information Processing Systems*, pages 5660–5670, 2017. Cited on page 23.
- A. G. d. G. Matthews, M. van der Wilk, T. Nickson, K. Fujii, A. Boukouvalas, P. León-Villagrà, Z. Ghahramani, and J. Hensman. GPflow: a Gaussian process library using TensorFlow. *Journal of Machine Learning Research*, 18(40):1–6, 2017. Cited on page 29.
- J. Moćkus. On Bayesian methods for seeking the extremum. In *Optimization techniques IFIP Technical Conference*, pages 400–404. Springer, 1975. Cited on page 30.

- M. Mutny and A. Krause. Efficient high dimensional Bayesian optimization with additivity and quadrature Fourier features. In *Advances in Neural Information Processing Systems*, pages 9005–9016, 2018. Cited on page 15.
- J. Nagumo, S. Arimoto, and S. Yoshizawa. An active pulse transmission line simulating nerve axon. *Proceedings of the Institute of Radio Engineers*, 50(10):2061–2070, 1962. Cited on page 33.
- H. Nickisch and C. E. Rasmussen. Approximations for binary Gaussian process classification. *Journal of Machine Learning Research*, 9:2035–2078, 2008. Cited on page 17.
- D. S. Oliver. On conditional simulation to inaccurate data. *Mathematical Geology*, 28(6):811–817, 1996. Cited on page 10.
- M. Oppner and C. Archambeau. The variational Gaussian approximation revisited. *Neural computation*, 21(3):786–792, 2009. Cited on page 18.
- A. Parker and C. Fox. Sampling Gaussian distributions in Krylov spaces with conjugate gradients. *SIAM Journal on Scientific Computing*, 34(3):B312–B334, 2012. Cited on page 19.
- G. Pleiss, J. R. Gardner, K. Q. Weinberger, and A. G. Wilson. Constant-time predictive distributions for Gaussian processes. In *International Conference on Machine Learning*, pages 4114–4123, 2018. Cited on pages 11, 19, 21.
- G. Pleiss, M. Jankowiak, D. Eriksson, A. Damle, and J. R. Gardner. Fast matrix square roots with applications to Gaussian processes and Bayesian optimization. In *Advances in Neural Information Processing Systems*, pages 22268–22281, 2020. Cited on page 19.
- J. Quiñero-Candela, C. E. Rasmussen, and C. K. I. Williams. Approximation methods for Gaussian process regression. In *Large-scale Kernel Machines*, pages 203–223. MIT Press, 2007. Cited on pages 18, 20, 29.
- A. Rahimi and B. Recht. Random features for large-scale kernel machines. In *Advances in Neural Information Processing Systems*, pages 1177–1184, 2008. Cited on page 12.
- C. E. Rasmussen and M. Kuss. Gaussian processes in reinforcement learning. In *Advances in Neural Information Processing Systems*, 2004. Cited on page 34.
- C. E. Rasmussen and J. Quiñero-Candela. Healing the relevance vector machine through augmentation. In *International Conference on Machine Learning*, pages 689–696, 2005. Cited on page 29.
- C. E. Rasmussen and C. K. I. Williams. *Gaussian Processes for Machine Learning*. MIT Press, 2006. Cited on pages 1, 10, 14, 16, 20.
- H. Rue and L. Held. *Gaussian Markov Random Fields: Theory and Applications*. CRC Press, 2005. Cited on pages 11, 31.

- H. Salimbeni, C.-A. Cheng, B. Boots, and M. P. Deisenroth. Orthogonally decoupled variational Gaussian processes. In *Advances in Neural Information Processing Systems*, pages 8711–8720, 2018. Cited on page 15.
- H. Salimbeni and M. P. Deisenroth. Doubly stochastic variational inference for deep Gaussian processes. In *Advances in Neural Information Processing Systems*, 2017. Cited on pages 37, 39.
- B. Schölkopf and A. J. Smola. *Learning with Kernels: Support Vector Machines, Regularization, Optimization, and Beyond*. MIT Press, 2001. Cited on page 12.
- M. Seeger. Bayesian methods for support vector machines and Gaussian processes. Technical report, 1999. Cited on page 18.
- B. Shahriari, K. Swersky, Z. Wang, R. P. Adams, and N. de Freitas. Taking the human out of the loop: a review of Bayesian optimization. *Proceedings of the IEEE*, 104(1):148–175, 2015. Cited on page 2.
- J. Shi, M. K. Titsias, and A. Mnih. Sparse orthogonal variational inference for Gaussian processes. In *Artificial Intelligence and Statistics*, pages 1932–1942, 2020. Cited on page 15.
- B. W. Silverman. Spline smoothing: the equivalent variable kernel method. *The Annals of Statistics*:898–916, 1984. Cited on pages 21, 23.
- B. W. Silverman. Some aspects of the spline smoothing approach to non-parametric regression curve fitting. *Journal of the Royal Statistical Society: Series B (Methodological)*, 47(1):1–21, 1985. Cited on page 20.
- E. Snelson and Z. Ghahramani. Sparse Gaussian processes using pseudo-inputs. In *Advances in Neural Information Processing Systems*, pages 1257–1264, 2006. Cited on page 18.
- J. Snoek, H. Larochelle, and R. P. Adams. Practical Bayesian optimization of machine learning algorithms. In *Advances in Neural Information Processing Systems*, pages 2951–2959, 2012. Cited on page 30.
- A. Solin and M. Kok. Know your boundaries: Constraining Gaussian processes by variational harmonic features. In *Artificial Intelligence and Statistics*, pages 2193–2202, 2019. Cited on pages 13, 31.
- A. Solin and S. Särkkä. Hilbert space methods for reduced-rank Gaussian process regression. *Statistics and Computing*, 30(2):419–446, 2020. Cited on page 13.
- P. Sollich and C. Williams. Using the equivalent kernel to understand Gaussian process regression. In *Advances in Neural Information Processing Systems*, pages 1313–1320, 2005. Cited on page 23.

- N. Srinivas, A. Krause, S. M. Kakade, and M. Seeger. Gaussian process optimization in the bandit setting: no regret and experimental design. In *International Conference on Machine Learning*, pages 1015–1022, 2010. Cited on page 30.
- D. Sutherland and J. Schneider. On the error of random Fourier features. In *Uncertainty in Artificial Intelligence*, pages 862–871, 2015. Cited on pages 12, 24, 25.
- W. R. Thompson. On the likelihood that one unknown probability exceeds another in view of the evidence of two samples. *Biometrika*, 25(3/4):285–294, 1933. Cited on page 30.
- M. E. Tipping. The relevance vector machine. In *Advances in Neural Information Processing Systems*, pages 652–658, 2000. Cited on page 20.
- M. Titsias and N. D. Lawrence. Bayesian Gaussian process latent variable model. In *Artificial Intelligence and Statistics*, pages 844–851, 2010. Cited on page 17.
- M. K. Titsias. Variational learning of inducing variables in sparse Gaussian processes. In *Artificial Intelligence and Statistics*, pages 567–574, 2009. Cited on pages 17, 18.
- M. K. Titsias. Variational model selection for sparse Gaussian process regression. Technical report, University of Manchester, 2009. Cited on page 17.
- M. van der Wilk, V. Dutordoir, S. T. John, A. Artemev, V. Adam, and J. Hensman. A framework for interdomain and multioutput Gaussian processes. *arXiv:2003.01115*, 2020. Cited on page 37.
- M. van der Wilk, C. E. Rasmussen, and J. Hensman. Convolutional Gaussian processes. In *Advances in Neural Information Processing Systems*, pages 2849–2858, 2017. Cited on page 37.
- C. Villani. *Optimal Transport: Old and New*. Springer, 2008. Cited on page 23.
- G. Wahba. *Spline models for observational data*. Society for Industrial and Applied Mathematics, 1990. Cited on page 20.
- K. Wang, G. Pleiss, J. Gardner, S. Tyree, K. Q. Weinberger, and A. G. Wilson. Exact Gaussian processes on a million data points. In *Advances in Neural Information Processing Systems*, pages 14622–14632, 2019. Cited on page 19.
- Z. Wang, C. Gehring, P. Kohli, and S. Jegelka. Batched large-scale Bayesian optimization in high-dimensional spaces. In *Artificial Intelligence and Statistics*, pages 745–754, 2018. Cited on page 15.
- P. Whittle. Stochastic processes in several dimensions. *Bulletin of the International Statistical Institute*, 40(2):974–994, 1963. Cited on page 31.

- A. Wilson and H. Nickisch. Kernel interpolation for scalable structured Gaussian processes. In *International Conference on Machine Learning*, pages 1775–1784, 2015. Cited on pages 11, 21.
- J. T. Wilson, V. Borovitskiy, A. Terenin, P. Mostowski, and M. P. Deisenroth. Efficiently sampling functions from Gaussian process posteriors. In *International Conference on Machine Learning*, pages 7470–7480, 2020. Cited on pages 23, 26, 29, 31.
- J. T. Wilson, F. Hutter, and M. P. Deisenroth. Maximizing acquisition functions for Bayesian optimization. In *Advances in Neural Information Processing Systems*, pages 9884–9895, 2018. Cited on page 30.
- A. T. Wood and G. Chan. Simulation of stationary Gaussian processes in  $[0, 1]^d$ . *Journal of Computational and Graphical Statistics*, 3(4):409–432, 1994. Cited on pages 11, 20.
- H. Zhu, C. K. Williams, R. Rohwer, and M. Morciniec. Gaussian regression and optimal finite dimensional linear models. Technical report, Aston University, 1997. Cited on page 13.
- D. L. Zimmerman. Computationally exploitable structure of covariance matrices and generalized covariance matrices in spatial models. *Journal of Statistical Computation and Simulation*, 32(1-2):1–15, 1989. Cited on page 11.